

Advective sorting of silt by currents: a laboratory study

Jeff Culp^{a,1}, Andrew Parent^b, Ehsan Abolfazli^a, Kyle Strom^{a,*}, Brian W. Romans^b

^aVirginia Tech, Civil and Environmental Engineering, Blacksburg, VA USA

^bVirginia Tech, Geosciences, Blacksburg, VA USA

Abstract

Accumulations of fine sediments along continental shelf and deep-sea bathymetric contours, known as contourite drifts, form a sedimentary record that is dependent on oceanographic processes such as ocean-basin-scale circulation. A tool used to aid in interpretation of such deposits is the sortable silt hypothesis, which suggests that the mean size of the sortable silt (silt from 10-63 μm) within a deposit can be used as a proxy for current velocity. While the hypothesis has been applied to numerous drift deposits, it has not been extensively explored. Slow deposition rates of contourite drift systems make it difficult to study in the deep ocean, and past laboratory studies have not tested the full range of conditions or mechanisms that could lead to sorting. This study uses flume experiments and theory to examine how the mean sortable silt in a deposit is related to current velocity under the action of advective depositional sorting. Tests were conducted for a fixed amount of time with four suspended sediment mixtures and current velocities typical of deep-sea settings (5-25 cm/s). Developed beds were sampled at fixed locations from the entrance and sized. The deposit grain size fined downstream and coarsened with increasing velocity at a particular distance from the inlet. Simple theory was able to capture the observations. Regardless of bed morphology or source sediment mixture, the mean sortable silt in the deposit was related to velocity at a particular flume location across all sediment mixtures. The slope of the relationship between velocity and size was dependent on the distance between the inlet and location of interest. Despite the simplified nature of the study, and the limitations regarding

*Corresponding author

Email address: strom@vt.edu (Kyle Strom)

¹Currently at: US Army Corps of Engineers District Office, Albuquerque, NM

the presumed variability in natural systems, these findings broadly support the validity of mean sortable as a proxy for paleocurrent velocity at a distance along a depositing current.

Keywords:

advective sorting, clay, contourite drift, silt, sortable silt

1. Introduction

Sedimentary deposits composed of particles $< 63 \mu\text{m}$ in size (i.e., mud/mudstone) make up the majority ($> 60\%$) of Earth's sedimentary record (Schieber, 1998), contain valuable archives of past environments and climate conditions (e.g., Knutz, 2008), and host important energy resources (e.g., Jarvie et al., 2007; Slatt, 2011). However, the physical processes that erode, transport, and deposit fine-grained sediment are still poorly understood compared to other sedimentary deposits (Schieber, 2011). Significant progress has been made over recent years demonstrating that clay ($< 4 \mu\text{m}$) can behave hydrodynamically similar to sand-size grains (e.g., bed load transport and associated bedform development) as a result of aggregation into larger, composite particles (up to 0.1-1.0 mm in size; Schieber et al., 2007); however, there has been comparably less focus on the silt fraction (4-63 μm). The 'sortable silt' proxy, which was developed by the palaeoceanography community to aid reconstruction of past deep-ocean current activity (McCave et al., 1995; McCave and Hall, 2006), provides a framework to further investigate fundamental questions pertaining to the way in which transport and deposition of silt could lead to sorting within a deposit under a specific set of conditions.

Currents in marine environments are responsible for the erosion, transport, and deposition of fine-grained sediment. In some areas, including coastal zones, continental shelves and shallow seas, and the deep ocean, significant accumulations of muddy deposits develop over geological timescales ($> 10^6$ yr) and, thus, represent archives of current history. For example, in the deep ocean, long-lived ocean-basin-scale boundary currents are a key component of global ocean circulation (Broecker et al., 1998) and have been linked to contourite 'drift' deposits that exceed a kilometre in thickness and extend for hundreds of kilometres (Heezen et al., 1966; Rebesco et al., 2014). Paleooceanographers

25 have been especially interested in reconstructing bottom-current history from contourite
26 drift deposits because of the linkage of abyssal currents to thermohaline circulation and
27 global climate. To aid in reconstruction, [McCave et al. \(1995\)](#) proposed a sedimentolog-
28 ical proxy for changes in current velocity that relate the size of non-cohesive silt to the
29 speed of the eroding or depositing flow. Specifically, [McCave et al. \(1995\)](#) hypothesized
30 that particles within the size range of 10 to 63 μm , defined as ‘sortable silt’ (SS), sort by
31 size with current velocity during selective deposition and selective erosion (winnowing)
32 (see [McCave and Hall, 2006](#), for a comprehensive review). Key statistics associated with
33 this size range that have been linked to velocity of ocean bottom currents include the
34 mean SS, SS_{mean} , and the SS percentage, $SS\%$ ([McCave and Andrews, 2019](#)).

35 Despite the widespread application of the SS hypothesis to deep-sea sediment core
36 samples of mostly Quaternary deposits (e.g., [Kleiven et al., 2011](#); [Thornalley et al., 2013](#)),
37 and some attempts at field calibration ([McCave et al., 2017](#)), the proxy remains largely
38 untested under controlled conditions. Slow deposition rates of contourites (2-10 cm/kyr)
39 make it difficult to robustly explore the hypothesis in the deep ocean, and the limited
40 number of laboratory studies that have been reported have not explored the full range of
41 possible conditions or mechanisms that could lead to sorting in the deep sea. In addition,
42 the general lack of knowledge regarding sediment transport and deposition mechanisms
43 in these systems highlights the need for fundamental experiments that isolate specific
44 processes. Only two known studies have sought to explicitly examine ideas related to
45 the SS hypothesis. The first, [Law et al. \(2008\)](#), set out to assess whether or not silt and
46 clay beds are subject to sorting through the process of selective erosion of fine grains.
47 Using core samples from the Gulf of Lions and a fluid shearing device known as a
48 Gust chamber, [Law et al. \(2008\)](#) found that sediment samples with less than 7.5% clay
49 were subject to erosional sorting via selective erosion (or winnowing), but that beds
50 with more than 7.5% clay were not susceptible to sorting. In cases with clay content
51 greater than 7.5%, the core surface tended to fail en masse rather than grain by grain.
52 The study highlighted the possibility of sorting by winnowing in non-cohesive beds
53 and the importance of clay (present and abundant in the majority of deep-sea drifts) in
54 modulating erosional sorting. However, the study did not examine sorting via selective

55 deposition.

56 Adding to the work of [Law et al. \(2008\)](#), [Hamm and Dade \(2013\)](#) used controlled
57 laboratory experiments conducted in a recirculating, oval-track flume to examine sorting
58 by a unidirectional current. Rather than focusing on selective erosion only, those authors
59 examined the use of SS as a proxy over current velocities that allowed for both deposition
60 and re-entrainment of previously deposited material in a current. In the experiment,
61 silt-sized glass spheres were used (diameters between 13-44 μm) for sediment, with no
62 clay-sized sediment added, and current velocities between 20 and 53 cm/s. For these
63 conditions, [Hamm and Dade \(2013\)](#) reported no evidence of significant sorting of grain
64 size within the bed as a function of current velocity. While these results did not confirm
65 the SS hypothesis originally proposed by [McCave et al. \(1995\)](#), [Hamm and Dade \(2013\)](#)
66 suggested that the study was not able to make any conclusions about the appropriateness
67 of the SS proxy under the conditions of advective down-current sorting of silt from a
68 sediment source due to the recirculating nature of the flume.

69 Both the [Law et al. \(2008\)](#) and [Hamm and Dade \(2013\)](#) studies have focused on
70 conditions that produce re-entrainment or erosion of bed material. Yet, it is likely that the
71 majority of deep-sea drift strata develops under largely depositional conditions (current
72 velocity < 25 cm/s). The field studies of [Ledbetter \(1986\)](#) and [McCave et al. \(2017\)](#)
73 suggest that size statistics in the silt range may indeed serve as a viable proxy for oceanic
74 bottom current velocity. Yet the velocity range over which their data suggests that there is
75 a correlation between velocity and silt size statistics is for $U < 25$ cm/s; a velocity range
76 that has not been tested experimentally. Furthermore, if the sampled deposits develop
77 under down-current dispersal of suspended sediment that originated from localized and
78 short-lived erosional events ([Richardson et al., 1993](#)), then it is possible that down-current
79 advective transport from a source may in fact be an important mechanisms of sorting (a
80 mechanism not examined in either [Law et al. \(2008\)](#) or [Hamm and Dade \(2013\)](#)).

81 The SS hypothesis stands as a valuable potential proxy for bottom current speed.
82 The laboratory study presented here focuses exclusively on one potential mechanism of
83 sorting. The mechanism we focus on is downstream advective sorting from a source of
84 suspended sediment under largely depositional conditions using sediment composed of

85 different mixtures of silt and clay. As such, a different mechanism of sorting is examined
86 under lower velocities than has been tested in past experiments. Specific aims of this
87 study are to examine whether or not the mean of the sortable silt within a deposit is
88 related to average current velocity, and to examine how any relationship that does exist
89 changes as a function of distance from the sediment input location. These aims are met
90 using laboratory flume experiments and simple theory. Both show support for the use of
91 SS as a proxy for current velocity in systems dominated by advection but does not take
92 into account sorting via winnowing. Thus, as part of this work, potential limitations of
93 these findings are also discussed with respect to deposits from natural systems.

94 **2. Methods**

95 *2.1. Approach*

96 This study seeks to investigate, via a flume study: (i) the functionality between
97 the mean SS, SS_{mean} , and current velocity, U , at a particular location; and (ii) how that
98 functionality changes with the distance from the sediment input location and the initial
99 composition of that sediment. The current velocities we are interested in correspond to
100 those primarily observed in oceanic bottom currents, i.e., $U = 0$ to 25 cm/s (McCave
101 et al., 2017). Velocities in this range are sufficient to move silt-sized material, but they
102 are generally insufficient to cause large scale erosion or pull material up into suspen-
103 sion (McCave et al., 1995; Niño et al., 2003; Hamm et al., 2009; Hamm and Dade, 2013).
104 Therefore, the experiments are net depositional with any sorting that occurs likely com-
105 ing from selective deposition or re-entrainment of freshly deposited grains rather than
106 erosion of a preexisting bed.

107 Laboratory studies using cohesive sediments and silts have been conducted in a
108 range different flume types, e.g., traditional recirculating laboratory flumes (Einstein
109 and Krone, 1962), annular flumes (Haralampides et al., 2003; Partheniades, 2006; Lau
110 and Krishnappan, 1992), enclosed shear chambers (Teeter, 1997; Law et al., 2008), race-
111 track flumes (Schieber et al., 2007; Hamm et al., 2009; Hamm and Dade, 2013; Yawar and
112 Schieber, 2017), and non recirculating flumes (Dixit et al., 1982). Each flume type has
113 its own set of strengths and weaknesses when it comes to studying the movement of

114 sediment. A traditional recirculating flume works well for sand and gravel studies, but
115 the high shear stress encountered in the pumps makes it less ideal for studying cohesive
116 sediment behaviour when flocculation could be an important process of consideration.
117 In addition, deposition of fine sediment within the flume system (flume, tailbox, pipes,
118 and headbox) makes it difficult to maintain a constant concentration at the flume in-
119 let (Mooneyham and Strom, 2018). Annular flumes are ring-shaped channels of water
120 that counter rotate to induce a constant shear across the bed of the flume. While an
121 annular flume can maintain constant shear over long periods of time without passing
122 sediment through pumps and pipes, it cannot be used to examine changes in the depo-
123 sition with distanced traveled from a source because the sediment in suspension keeps
124 getting wrapped around the same section of bed. Oval-shaped 'racetrack' flumes are
125 similar in that no pumps or pipes are involved and material is continuously moved
126 around a closed circuit. Such systems work well for developing equilibrium conditions
127 between deposition and erosion, but they also do not allow for examination of how the
128 distance from the input alters the nature of the deposit. Taking these limitations into con-
129 sideration, a linear flow-through flume was chosen here in which no water or sediment
130 is recirculated back to the inlet. While this type of flume is resource intensive, it does
131 allow for a constant upstream concentration boundary condition and the development
132 of spatial patterns in the deposit.

133 Four different sediment mixtures (pure clay, pure silt, 2:1 silt to clay and 1:1 silt to
134 clay) were used in the experiments. In all cases, a well-mixed suspension of water and
135 sediment was fed at a constant rate at the upstream end of the flume. Beds developed
136 downstream with spatially varying patterns as sediment deposited from flow. The de-
137 posited bed that remained at the end of each experiment was then sampled at 1.52 m (5
138 ft) increments from the inlet and measured with a SediGraph 5120 particle size analyzer
139 (Micromeritics, Norcross, GA, USA) to allow for calculation of SS_{mean} . Current velocities
140 for the experiment ranged from 5 to 25 cm/s.

141 2.2. *Depositional theory*

142 This section develops simple theory to predict the size distribution of silt in a de-
 143 posit and thereby an initial prediction regarding the behaviour of $SS_{mean} = SS_{mean}(x, U)$.
 144 Comparing the experimental results to the theory provides the opportunity to extend
 145 the laboratory results to larger scales if the model is found to describe the data well. The
 146 model also can be used to help inform what processes are important to consider if the
 147 experimental data deviates from the expectation set by the simplified theory.

148 The context of the model is that of depositional sorting in a boundary layer flow.
 149 As such, the model's foundation is provided by the one-dimensional (layer-averaged)
 150 advection-dispersion equation for suspended sediment of grain size fraction i :

$$151 \quad \frac{\partial(AC_i)}{\partial t} + \frac{\partial(AUC_i)}{\partial x} = \frac{\partial}{\partial x} \left(AK_x \frac{\partial C_i}{\partial x} \right) + b(E_{b,i} - D_{b,i}) \quad (1)$$

152 where A is the cross sectional flow area of the current containing sediment, b is current
 153 width, C_i is the layer-averaged volume concentration of suspended sediment (the total
 154 concentration is $C = \sum C_i$), K_x is the dispersion coefficient, $E_{b,i}$ is an erosive flux and $D_{b,i}$
 155 is a depositional flux for grain size fraction i across the sediment-water interface.

156 Assuming steady, uniform hydraulics and a rectangular or top-hat current cross-
 157 sectional area with a constant sediment input, Eq. 1 simplifies to:

$$158 \quad bhU \frac{\partial C_i}{\partial x} = b(E_{b,i} - D_{b,i}) \quad (2)$$

159 Here h is the flow thickness with the cross-sectional flow area being defined as $A = bh$.
 160 The solution of Eq. 2 yields $C_i = C_i(x)$ if models for the deposition and erosion flux
 161 are specified. Typically the maximum deposition flux for grain size fraction i is taken to
 162 be $D_{b,i} = \alpha_i w_{s,i} C_{b,i}$, where $w_{s,i}$ is the settling velocity for size i and $C_{b,i}$ is the near-bed
 163 concentration of size fraction i ; α_i can be thought of as the ratio of the true depositional
 164 velocity of size fraction i divided by the still water settling velocity, $w_{s,i}$. $E_{b,i}$ is often
 165 modeled as $E_{b,i} = w_{s,i} E_{s,i}$ where $E_{s,i}$ is a dimensionless erosion or entrainment velocity.

166 To solve Eq. 2, constant values or closure equations are needed for α_i and $E_{s,i}$. When
 167 the particle diameter is less than the thickness of the viscous sublayer, the experiments of
 168 [Hamm et al. \(2009\)](#) suggests that α_i and $E_{s,i}$ are both controlled by the ratio of the viscous

169 lift to the particle's gravitational body force. In such cases, the analytical solution for
 170 viscous lift given by Saffman (1965) for small particle Reynolds numbers yields a ratio
 171 of these two forces that is proportional to $u_*^3/(g'\nu)$; here u_* is the friction velocity and
 172 $g' = gR_s$ with R_s being the submerged specific gravity of the sediment ($R_s = 1.65$).
 173 Hamm et al. (2009) referred to this ratio as the Saffman parameter, $S \equiv u_*^3/(g'\nu)$. The
 174 analytical expression for the gravitational and lift forces are both dependent on particle
 175 diameter. However, both forces are proportional to d^3 , resulting in the ratio of the forces
 176 being independent of particle size. Based on curve fitting, Hamm et al. (2009) found that
 177 their experimental data was best described with:

$$178 \quad \alpha = 1 - S \quad (3)$$

$$179 \quad E_s = S^{5/2} \quad (4)$$

181 For the simplified model used here, Eqs 3 and 4 are adopted, resulting in size-
 182 independent α_i and $E_{s,i}$ values. Assuming a well-mixed condition for suspended sed-
 183 iment over the thickness of the turbid boundary layer ($C_{b,i} = C_i$), the deposition and
 184 entrainment fluxes become:

$$185 \quad D_{b,i} = \alpha w_{s,i} C_i \quad (5)$$

$$186 \quad E_{b,i} = w_{s,i} E_s \quad (6)$$

188 Therefore, the net rate of deposition to, or accumulation in, the bed of sediment of size
 189 fraction i is:

$$190 \quad D_{b,i} - E_{b,i} = w_{s,i}(\alpha C_i - E_s) \quad (7)$$

191 Using the rate of accumulation, the total fraction of the bed material of size i can be
 192 defined as:

$$193 \quad f_{b,i} = \frac{w_{s,i}(\alpha C_i - E_s)}{\sum w_{s,i}(\alpha C_i - E_s)} \quad (8)$$

194 Values of $f_{b,i}$ as a function of distance are what one needs to develop predictions for the
 195 spatial arrangement of SS_{mean} in the flume or a boundary current. $f_{b,i} = f_{b,i}(x)$ can be
 196 obtained from the solution of Eq. 2 using Eqs 5 and 6 for the exchange rates of material
 197 at the water-sediment interface. The result is:

$$198 \quad C_i = \left(C_{i,0} - \frac{E_s}{\alpha} \right) e^{-\frac{\alpha w_{s,i}}{U} \left(\frac{x}{h} \right)} + \frac{E_s}{\alpha} \quad (9)$$

199 In Eq. 9, x/h is the scaled downstream distance. Assuming consistency between $\alpha w_{s,i}/U$
 200 in the laboratory and field, the scaled downstream distance becomes the primary ratio
 201 for mapping the calculations from the laboratory scale to the field. Alternatively, the
 202 ratio of $hU/(\alpha w_{s,i})$, or the horizontal advective length scale for sediment of size i , $L_i =$
 203 $hU/(\alpha w_{s,i})$, can also be used in Eq. 9 to scale the downstream distance:

$$204 \quad C_i = \left(C_{i,0} - \frac{E_s}{\alpha} \right) e^{-\frac{x}{L_i}} + \frac{E_s}{\alpha} \quad (10)$$

205 When coupled with a settling velocity equation (e.g., [Ferguson and Church, 2004](#)),
 206 the model (Eqs 8 and 9 or 10) predicts the silt size distribution in the bed as a function of
 207 the distance from the input, x , the current velocity, U , the current thickness, h , the size
 208 distribution of the source material, and the Saffman parameter (or u_* , which the authors
 209 link to U). An implicit assumption embedded in the model is that deposited material is
 210 immobile; that is, the model does not account for bed load transport.

211 This simplified model was used to examine $f_{b,i} = f_{b,i}(x, U)$ and the resulting
 212 $SS_{mean} = SS_{mean}(x, U)$ over the x and U values expected in the experiments (Figs 1
 213 and 2); the exact definition of SS_{mean} is given in the *Calculation of the mean sortable silt*
 214 section. These calculations were made using: (i) a synthetic initial SS size distribution
 215 based on the input sediment; and (ii) the $u_* = u_*(U)$ relation from these experiments.
 216 The synthetic SS distribution reasonably mimics the average SS size distribution used
 217 in the experiments and was developed assuming that the natural log transformed grain
 218 sizes are normally distributed with a mean of $\theta_m = 3.2$ (24.5 μm) and a standard deviation,
 219 $\sigma = 0.8$ ($\theta_m - \sigma = 11$ μm and $\theta_m + \sigma = 54.5$ μm). For context, u_* values from these
 220 experiments produced Saffman numbers between 0.002 to 0.15, and therefore α values
 221 ranging from 1 to 0.85 with $E_s \approx 0$.

222 The model predicts a decrease in SS_{mean} with distance from the flume inlet (or
 223 source of suspended sediment), x , as one would expect for downstream fining under
 224 advective sorting (Fig. 1). Increases in either h or U result in coarsening at a given
 225 location (Eq. 9) as a result of the increase in the advective length scale, L_i ; doubling
 226 either h or U produces a doubling of L_i . For fixed x (that is, at a station) and h , SS_{mean}
 227 increases with U (Fig. 2). The model predicts that the relationship between SS_{mean} and

228 U becomes more linear with increased distance from the input (Fig. 2). In addition, the
229 slope of the SS_{mean} and U relation first increases with distance and then decreases as
230 grain sizes available for deposition become depleted (Fig. 2). The outcome of this simple
231 analysis suggests that a linear relationship between the average silt size (Ledbetter, 1986)
232 or SS_{mean} (McCave et al., 2017) might apply best to locations farther away from the initial
233 sources of suspended sediment if advective sorting is responsible for the building the
234 deposit.

235 2.3. Experimental equipment and materials

236 All experiments were conducted in a 18 cm wide, 9.14 m long, tilting acrylic flow-
237 through flume (Fig. 3). The inflow for the system is controlled with a constant-head
238 tank and valve on the inflow line. Water from the constant-head tank is discharged to
239 a mixing tank, where sediment is added via a calibrated AccuRate dry material feeder.
240 The suspension then flows from the mixing tank to the flume headbox, through the flow
241 straighteners, down the length of the channel, and into a settling basin before being
242 discharged to the drain. Uniform flow is maintained over the length of the channel
243 through adjustment of the channel slope and a series of removable vertical bars at the
244 flume outlet. The maximum amount of flow that can be put through the system is
245 dependent on the volume in the storage tank, the volume flow rate of water that can be
246 added to the storage tank, and the capacity of the drain line in the laboratory. Taken
247 together, the maximum flow velocity that can be sustained with the system is 28 cm/s
248 at a flow depth of 3.4 cm for 2 hours, which yields a maximum functional discharge of
249 1.7 L/s.

250 Other equipment used in the experiments included an overhead camera (Canon
251 80D; Canon, Tokyo, Japan) attached to a sliding rail and Campbell Scientific Optical
252 Backscatter Sensors (OBS; Campbell Scientific Limited, Loughborough, UK) 3+ probes
253 (Fig. 3). The camera was used during the experiments to observe, when possible, the
254 development and movement of the bed through video and time-lapse photography. The
255 camera was also used to develop a mosaic of the entire bed after water had been drained
256 from the flume at the completion of each run. The OBSs were installed at the up and

257 downstream ends of the flumes for a subset of runs to monitor concentration. These
258 were calibrated beforehand using each of the sediment mixtures over a large range of
259 concentrations. All regressions for the OBSs were done with 18 or more points, and R^2
260 values for each exceeded 0.99.

261 The sediment used in the experiments included crushed silica (silt) sourced from
262 US Silica under the name SIL-CO-SIL, kaolinite supplied by Georgia Kaolinite, and a
263 100% non-treated sodium bentonite of the name Aquagel Gold Seal. Four mixtures were
264 tested at varying flow velocities: 100% silica silt, 5:4:1 silica silt:kaolinite:bentonite, 5:8:2
265 silica silt:kaolinite:bentonite, and 4:1 kaolinite:bentonite. These sediment mixtures will
266 hereafter be referred to as pure silt, silt to clay 1:1, silt to clay 1:2, and pure clay respec-
267 tively. These clay:silt ratios resemble the range observed in muddy and silty contourites
268 (Rebesco et al., 2014; McCave and Hall, 2006) as well as those tested in flocculation ex-
269 periments that found silt to entrain into flocs in a depositional environment (Tran and
270 Strom, 2017); the type of bentonite used in the present study is different from that of
271 Tran and Strom (2017). Grain size distributions of the input sediment mixtures used for
272 each experiment can be seen in Figure 4.

273 Each experiment proceeded by setting the discharge to the desired rate, checking
274 for the development of uniform flow in the channel and adjusting the number of bars
275 at the flume exit as needed, followed by engagement of the sediment feeder. All experi-
276 ments were run for a duration of 2 hours. Through preliminary experiments 2 hours was
277 determined to be a sufficient amount of time to accumulate enough sediment in the bed
278 for sampling. The conditions used in the experimental matrix are given below following
279 a discussion on results from a set of preliminary tests.

280 Flow velocity, U , was calculated for each run using the measured volumetric dis-
281 charge, Q , the measured flow depth, h , and known flume width, w , as $U = Q/(hw)$.
282 Shear velocity, u_* , values for each case were obtained by solving the smooth-wall Keule-
283 gan resistance equation,

$$284 \frac{U}{u_*} = \frac{1}{\kappa} \ln \left(\frac{hu_*}{\nu} \right) + 5.5 - \frac{1}{\kappa} \quad (11)$$

285 where, $\kappa = 0.4$ is the von Karman constant and ν is the kinematic viscosity of the water.
286 The bed shear stress, τ_B is related, by the definition of the friction velocity, as $\tau_B = \rho u_*^2$.

287 *2.4. Flocculation potential of the sediment mixtures and the role of clay hydration time and*
288 *salinity in the experiments*

289 The flocculation behaviour of the various mixtures that included clay was tested
290 in a separate set of flocculation mixing-tank experiments similar to those conducted by
291 [Tran and Strom \(2017\)](#). In the mixing-tank experiments, the size distribution of the ma-
292 terial in suspension is measured as a function of mixing time using a specially designed
293 microscope system that allows for measurement of particles and flocs in suspension
294 without removing samples from the tank (see [Tran and Strom \(2017\)](#) for details). The
295 purpose of the mixing-tank experiments was to determine if the flocculation potential
296 of the sediment was strongly influenced by: (i) the wetting time of the clay prior to be-
297 ing introduced to the flume; and (ii) the presence or absence of salt. The experimental
298 parameters investigated included: sediment type (the silt and kaolinite mix with and
299 without the bentonite), wetting time (a short wetting time and a 24 hr wetting time), and
300 salinity (0 and 5 ppt). This set of parameters resulted in eight mixing-tank experiments.
301 The short wetting time samples were obtained by turning on the flume, sediment feeder,
302 and water-sediment mixing system at the rates used in the flume experiments, collecting
303 samples of suspended sediment issuing from the flume inlet, and then transferring those
304 samples to the flocculation mixing tank. The 24 hr hydration samples were collected in a
305 similar way but were left to sit in the mixing tank water for 24 hours before starting the
306 mixer to observe flocculation. For each experiment, the mixer was set as low as possible
307 while still being able to maintain the material in suspension. Size distributions of the
308 material in suspension were recorded every minute for two hours (sample images from
309 the experiments can be found in the supplemental material).

310 For all experiments, particles and aggregates consisting of clay and silica were
311 present in suspension. However, no significant flocculation was observed in any exper-
312 iment. The size distributions of the suspensions were consistent both through time in
313 each experiment and across all experiments. Clay in suspension did exist in a range
314 of aggregate sizes, but these aggregates were small and more compact than the more
315 loosely bound flocs of [Tran and Strom \(2017\)](#). Furthermore, no binding of the silica
316 silt particles in the clay aggregates was observed. Samples extracted near the bed and

317 imaged with the microscope system from two of the flume experiments showed similar
318 sized material and a general lack of large, low-density flocs capable of binding up silt
319 particles. Based on the mixing-tank experiments, it is concluded that the clay and silt
320 mixtures emanating from the flume inlet would not be significantly different if the sedi-
321 ment mixture was pre-hydrated for more time or salt was added to the water. Knowing
322 this is advantageous because of the difficulty involved with wet feeding a saline, uniform
323 sized suspension of material over the course of two hours. In addition, the experiments
324 show that the potential for silt particles to bind within clay flocs is low for these partic-
325 ular sediment mixtures.

326 *2.5. Deposit sampling and grain-size measurement*

327 Bed samples were collected at the end of each 2-hr experiment after most of the
328 water in the flume had been carefully drained from the flume. Samples were collected
329 at five stations at distances of 1.52 m (5 ft), 3.05 m (10 ft), 4.57 m (15 ft), 6.10 m (20
330 ft), and 7.62 m (25 ft) from the inlet (Fig. 3). To ensure the capture of all of the fine
331 sediment, the samples were collected using a large syringe over a 5 cm x 5 cm patch of
332 bed (or an area large enough to sample a minimum of 1 g of sediment by dry weight).
333 Each sample contained both sediment and water. These samples were stored in labelled
334 vials for sizing at a later time and the syringe was flushed with clean water several times
335 between each sample to ensure that samples from a given site were not contaminated
336 with remnant grains from a different location or experimental run.

337 The grain size distribution of each bed sample was measured using a Micromerit-
338 ics SediGraph 5120. The SediGraph is a reliable instrument for measuring the grain
339 size distribution of fine-grained sediments (e.g., [Bianchi et al., 1999](#)) and has been used
340 extensively for SS proxy applications. The SediGraph calculates grain size distribution
341 using x-rays to measure sediment concentration and settling velocity, which is then used
342 to compute grain size using Stokes' Law:

$$343 \quad d = \left(\frac{18w_s v}{g'} \right)^{1/2} \quad (12)$$

344 Once bed samples were collected, water was decanted and bulk sediment was dried for
345 48 hr. Once samples were sufficiently dried, a 1.0 g split was separated for analysis in

346 the SediGraph. The split was dispersed in 65 mL of analysis fluid: ultra-pure (18.2 Ω
 347 m resistivity) water for pure silt samples and 0.5% tetrasodium pyrophosphate (TSPP)
 348 ultra-pure water for samples containing clay, to reduce particle flocculation during anal-
 349 ysis. Samples dispersed in TSPP underwent a 15 min ultrasonic bath to further eliminate
 350 flocculation of the sample.

351 2.6. Calculation of the mean sortable silt

352 SS_{mean} was calculated from the natural log transformed bin sizes, $\theta_i = \ln(d_i)$ where
 353 d_i is the percent finer than bin edge in microns used in the process of measuring and
 354 quantifying the total grain size distribution of a sample (e.g. a SediGraph output). SS_{mean}
 355 is defined as:

$$356 \quad SS_{mean} = e^{\theta_m} \quad (13)$$

357 with θ_m defined as,

$$358 \quad \theta_m = \sum_{i=1}^n \bar{\theta}_i f_{ss,i} \quad (14)$$

359 where $\bar{\theta}_i$ is equivalent to the “natural log of the bin’s geometric mid-point diameters”,
 360 $\bar{\theta}_i = (\theta_i + \theta_{i+1})/2$ (McCave and Andrews, 2019), and $f_{ss,i}$ is the fraction of material
 361 associated with the SS size range (10 to 63 μm) in bin i . $i = 1$ is associated with the bin
 362 whose lower edge is 10 μm ; $i = n$ is associated with the bin whose upper edge is 63 μm :
 363 $f_{ss,i} = p_i / \sum_{i=1}^{i=n} p_i$.

364 2.7. Defining the experimental conditions

365 A series of preliminary experiments were run to determine the general repeatabil-
 366 ity of the methods and the influence of inlet sediment concentration, flow depth, and
 367 experimental runtime on the SS_{mean} in the deposit for the purpose of defining the fi-
 368 nal experimental conditions. Repeat 2 hr experiments, even at different concentrations,
 369 generally showed less than $\pm 1 \mu\text{m}$ variation between any individual SS_{mean} statistic at a
 370 given sampling location. This suggests that the experimental methods show little varia-
 371 tion in SS_{mean} from run to run. The one exception to this was that up to 1.4 μm variation
 372 was observed at the most distal location (Fig. 5A). The fact that the variability between
 373 SS_{mean} at a given location under different inlet concentrations ($C \approx 500$ and 1000 mg/L)

374 was also in the same variation range indicates that the deposit grain size distribution
375 is not dependent on the inlet concentration. Inlet concentration does significantly influ-
376 ence the deposition rate, but it does not fundamentally change the size distribution in
377 the deposit. This result is advantageous because it allows for running experiments at
378 concentrations higher than would be expected in a natural boundary current to speed
379 up time without altering the size distribution in the deposit. It also means that varia-
380 tions in concentration at the inlet should not impact the results. The lack of dependence
381 of grain size in the deposit on source concentration is also helpful for modelling since
382 initial concentration data following an episodic resuspension event is sparse.

383 This study also examined the role of flow depth, h , on the deposit grain size distri-
384 bution and resulting SS statistics (Fig. 5B). Unlike concentration, changes in flow depth
385 do produce significant differences in SS_{mean} at a given distance downstream of the input
386 all else being constant (e.g., constant velocity and input sediment size characteristics).
387 This is to be expected given the dependence of $C_i = C_i(x)$ on the ratio $\alpha w_{s,i}/(hU)$ (Eq. 9).
388 In the simple depositional model, h has as significant of influence on the concentration
389 profile as U . In general, increasing flow depth coarsens the deposit at a given location
390 due to the increase in the advection length scale of a given particle size $L_i = hU/(\alpha_i w_{s,i})$
391 (Fig. 5B). Because this study is interested in the relationship of $SS_{mean} = SS_{mean}(x, U)$,
392 depth was held constant at $h = 3.4$ cm in all other experiments. Using this depth, the ex-
393 perimental Reynolds number, $Re = Uh/\nu$ ranged from 1500 to 9000 (low but turbulent).

394 If particles that deposit from the current to the bed do not move, then the grain
395 size distributions in the beds will be independent of experimental duration. However,
396 in these experiments, some of the deposited particles did move as bed load, and the
397 downstream movement intensified with increasing velocity. The presence of bed load
398 suggests that the size of the sediment in the beds at a given distance down channel
399 could change with the total runtime of the experiment. The sensitivity of the measured
400 SS_{mean} to variations in experimental run time was tested by comparing results between
401 a standard experimental run time of 2 hr to an experiment with a run time of 6 hr
402 (Fig. 5C). The differences in SS_{mean} between these two experiments at the three upstream
403 sampling locations all fell within the range of experimental variability. However, slight

404 coarsening of SS_{mean} ($\approx 1 \mu\text{m}$) at the two most distal locations was observed (Fig. 5C).
405 This is attributed to downstream transport via bed load motion of larger grains sizes.

406 Given that experimental run time could impact the distribution of SS, the run time
407 for all experiments was fixed at 2 hr and varied the inlet concentration to ensure that
408 enough sediment deposited during the 2 hr to be sampled and sized with the SediGraph.
409 Flow depth was fixed at 3.4 cm for all runs, and velocity was varied from 5 to 25 cm/s
410 (Table 1). Taken together, these conditions and procedures enable isolation of the link
411 between SS_{mean} , flow velocity, and distance from the input for each of the four sediment
412 mixtures. The scaled distance over which the deposits in the flume develop is from
413 $x/h = 0$ to ≈ 260 , which is equal to a corresponding distance of 0 to 26 km for a 100 m
414 thick boundary current.

415 3. Results

416 3.1. Transport conditions

417 The key hydraulic and sediment transport parameters associated with each of the
418 five experimental velocities are first presented for the purpose of contextualizing the
419 conditions before describing the bed morphology or $SS_{mean} = SS_{mean}(x, U)$ results. The
420 flow parameters presented are: the shear velocity, the bed shear stress, a measure of
421 the thickness of the initial viscous sublayer, $\delta = 5\nu/u_*$, and the Saffman parameter,
422 S . Two other sediment transport ratios are also provided for silt sizes 10, 30, and 60
423 μm . The two ratios are u_*/w_s , a measure of how well mixed particles in suspension are
424 over the vertical, and τ^*/τ_{cr}^* , a measure of particle mobility or transport intensity for
425 those particles that make it to the bed. For the transport intensity parameter, τ^* is the
426 dimensionless bed shear stress ($\tau^* = u_*^2/u_g^2$) and τ_{cr}^* is the value of the dimensionless
427 shear stress where significant bed load motion occurs. Here the τ_{cr}^* threshold was calcu-
428 lated as $\tau_{cr}^* = [0.22Ga^{-0.6} + 0.06 \exp(-17.77Ga^{-0.6})]/2$ where Ga is the Galileo number,
429 $Ga = u_g d/\nu$ (a type of particle Reynolds number, (e.g. Charru and Hinch, 2006)), with u_g
430 being the particle velocity scale associated with the submerged gravitational body force,
431 $u_g = \sqrt{g'd}$ (García, 2008). The equation for τ_{cr}^* yields the classic Shields curve divided by
432 2. This reduced Shields threshold was chosen since it predicted motion for cases where

433 $U \geq 15$ cm/s, which is in line with the observations in this study. All of the contextual
434 parameter and ratio values are given in Table 2.

435 Values of u_*/w_s indicate transport in the downstream direction being dominated
436 by suspended load, $u_*/w_s > 1$, and, at least for the $d = 10$ and $30 \mu\text{m}$ cases, being
437 fairly well mixed over the vertical, $u_*/w_s > 6$; which is equivalent to a Rouse number of
438 $Z_R = w_s/(\kappa u_*) < 0.4$ (García, 2008). Nevertheless, all runs except for the case of $U = 25$
439 cm/s with pure clay experienced deposition and the development of a bed that could be
440 sampled at at least two locations in the flume.

441 In all runs, the thickness of the viscous sublayer exceeded the diameter of the silt in
442 the mixture by a factor of roughly 10 (i.e., $\delta > 400 \mu\text{m}$). This suggests that any sediment
443 that made it to the boundary would be submerged in the region of flow dominated
444 by viscous effects. In such cases, the likelihood of re-entrainment of particles from the
445 wall region can be quantified with S (Saffman, 1965; Hamm et al., 2009); Saffman (1965)
446 proposed a value of $S = 0.65$ is needed for the average viscous lift force to overcome
447 the gravitational force on a particle. The highest value of S was ≈ 0.15 . The authors
448 therefore expect that most of the particles that make it to the bed will likely remain in
449 the near bed region rather than being resuspended up into the flow.

450 While the Saffman values suggest that experimental conditions are in line with a
451 net depositional setting for silt, it is still possible for particles on the bed to move in the
452 downstream direction as bed load. The ratio of τ^*/τ_{cr}^* provides a measure of the flows
453 ability to move particles on the bed with values greater than 1 suggesting motion. In
454 all experiments with silt, the onset of bed load was found to be well captured by this
455 ratio. For runs with $U < 15$ cm/s, the bed that developed was largely immobile and
456 topographically featureless. However, for all runs containing silt in the input sediment
457 and $U \geq 15$ cm/s, active bed load occurred throughout the experiment and led to
458 the development of migrating bedforms similar to those of Mantz (1978), Hollister and
459 McCave (1984), Hamm and Dade (2013), and Yawar and Schieber (2017).

460 3.2. Bed morphology

461 The deposit thickness, morphology, and grain size all varied spatially down the
462 flume and with flow velocity. A constant spatial trend in all cases was that the deposit
463 thickness decreased in the downstream direction. When silt was present and $U \geq 15$
464 cm/s, the bed morphology transitioned downstream from a flat deposit with a few
465 moving particles in the surface layer, to migrating two-dimensional (2D) ripples, and
466 then to migrating barchan shaped three-dimensional (3D) ripples. A similar patten of a
467 featureless deposit, to 2D ripples, to barchan ripples was also observed at a given station
468 with increases in velocity. Both trends in morphology are interpreted as an outcome of
469 a reduction in the amount of silt in the bed load layer with distance from the inlet and
470 with increased velocity at a station. Input material also influenced the type and size of
471 bedforms present. Increases in clay content moved the transition from a flat bed to 2D
472 ripples, or from 2D ripples to barchan ripples, farther downstream (Figures 6-10).

473 At a flow velocity of 5 cm/s (Fig. 6), no bedforms were observed with any of the
474 four inlet sediment mixtures. Instead, deposition resulted in a smooth, uniform bed
475 throughout the length of the flume. At a flow velocity of 10 cm/s (Fig. 7), bedforms are
476 minimal with some small (< 1 cm wavelength) 2D ripples being apparent in the pure
477 silt runs, but no true ripples forming in any run with clay.

478 At $U = 15$ cm/s (Fig. 8), 1-2 mm tall ripples were present at the first three sampling
479 locations in all experiments containing silt; ripples were not present in the pure clay
480 experiment. The pure silt experiment saw a continuation of these ripples to the end of
481 the flume, while the experiment with clay saw the ripples transition into barchan ripples
482 around 6.4 m for the 1:1 experiment, and around 5.5 m for the 1:2 experiment.

483 At $U = 20$ cm/s, pure silt beds transitioned from 2D ripples to barchans moving
484 downstream (Fig. 9). A similar pattern occurred for the clay and silt experiments, with
485 the structures becoming more disorganized as clay content increased. Pure clay resulted
486 in no bedforms with only a few bare patches in the bed followed downstream by a zone
487 of no net accumulation of sediment. Bed load did occur in the form of what have been
488 called floccule streamers (Schieber et al., 2007) in the zone of no net accumulation (Fig.
489 9, lower right). The streamers convey sediment parallel to the flow direction within

490 low-speed streaks and were visually evident in all experiments. Increasing velocity to
491 25 cm/s (Fig. 10) resulted in an increase in height of the pure silt barchans (up to 8 mm,
492 $h/h_{\text{bedform}} = 4.25$). Bedforms in the clay and silt mixtures became increasingly sparse.
493 Large clay aggregates, likely an artifact of the mixing process, were also mobile at this
494 velocity and were able to move as bed load down the flume, some of which deposited in
495 the stoss and lee sided of the ripples. A thin deposit of these clumps was also observed
496 from 0-3.8 m along the flume. The experiment with pure clay did contain bed load
497 transport but yielded no net deposition.

498 3.3. Downstream patterns in deposit grain size

499 All of the experiments using silt, regardless of the amount or type of clay added,
500 exhibited some degree of systematic downstream fining of the SS fraction in the bed (Fig.
501 11). Downstream fining was stronger (more change in the bed size distribution for each
502 step in distance downstream from the inlet) for the lower velocities than it was for higher
503 velocity (Fig. 11). In fact, for some of the 25 cm/s runs, little change was observed in
504 the deposit grain size distribution. This result could be interpreted as the system either
505 needing longer distances to observe the fining or the system pushing more towards an
506 equilibrium state between deposition and re-entrainment as velocities increase.

507 The size distribution data in Figure 11 also shows that the distribution of SS at
508 a given station coarsens with current velocity. This can be observed by comparing the
509 cumulative distribution curves at $x = 4.57$ m in the top row of the figure for velocities
510 of 5, 15, and 25 cm/s. Because the conditions are overall net depositional ($E_s \approx 0$), the
511 coarsening with the increase in velocity can be interpreted as the outcome of an increase
512 in the advective length scale, L_i , (Eq. 10).

513 3.4. The relationship between sortable silt and current velocity at a station

514 SS_{mean} was calculated following the method described in the *Calculation of the mean*
515 *sortable silt* section for every bed sample for which silt was present in the input sediment
516 (i.e., for all runs except the pure clay runs). The range of SS_{mean} across all experiments
517 and station locations was 15 to 45 μm . SS_{mean} systematically decreases progressing from
518 the flume entrance to exit following a trend similar to the d_{50} of the SS fraction (Fig. 11).

519 All SS_{mean} data were grouped by station and plotted against current velocity to ex-
520 amine the relationship between SS_{mean} and U (Fig. 12). Linear regression was performed
521 with SS_{mean} as the scalar response and U as the explanatory variable at each station. The
522 regression was performed for data for each sediment type independently and also for
523 a combined dataset using SS_{mean} values from all three sediment mixtures. The fit equa-
524 tions for the combined dataset are shown in Figure 12; the coefficients and R^2 values
525 for all regressions are given in Table 3. Of the four sets of regression coefficients, those
526 obtained from the combined dataset have been chosen here (i.e., Fig. 12 and the “All”
527 rows in Table 3) to be the most significant since they were developed with the largest
528 number of data points. For these regressions, R^2 ranges from 0.7 to 0.94 (Table 3).

529 Three trends are evident in the regression output. The first is that the data tend
530 to be better described by linear regression as the distance from the flume inlet increases
531 (Fig. 12). The second and third are that the slope of the fit line increases with distance
532 from the inlet (from 0.54 to 0.8) and the intercept decreases (from 23.8 to 13.2).

533 While not shown in the figures or tables, a regression was also performed between
534 SS_{mean} and the shear velocity, u_* . For this particular set of data, no predictive power was
535 gained by using u_* instead of U . For this reason, and because the classic SS hypothesis
536 relates SS_{mean} and velocity, the discussion focuses on the relationship between SS_{mean} and
537 velocity rather than shear velocity or bed shear stress.

538 4. Discussion

539 Before discussing the results, it is important to highlight that this study only has
540 the ability to examine $SS_{mean} = SS_{mean}(x, U)$ under the action of downstream advective
541 sorting in a depositional environment with minimal to no bed load transport. Further-
542 more, because the flocculation potential of the sediment mixture was low, the results
543 presented reflect conditions unaffected, or minimally affected, by flocculation. Addi-
544 tional discussion of the study limitations and results context are given below following
545 the discussion of the results.

546 4.1. Comparison with field and other laboratory data

547 A primary outcome of the study is the experimental demonstration that silt in
548 a depositional system does sort advectively both downstream and at a station as a
549 function of velocity over the range of $U = 5$ to 25 cm/s. Within this context, it is found
550 that grain size sorting is dependent on the distance from the flume inlet to the sample
551 location and the flow depth; an additional analysis discussed below also shows that
552 it is dependent on the size distribution of the sediment at the source or inlet location.
553 Furthermore, under the present experimental conditions, SS_{mean} appears to be linearly,
554 or nearly linearly, related to the average current velocity at a particular distance from the
555 flume inlet.

556 The studies of [Ledbetter \(1986\)](#) and [McCave et al. \(2017\)](#) provide the only known
557 field data examining the relationship between the mean silt ([Ledbetter, 1986](#)) and SS
558 ([McCave et al., 2017](#)) and current velocity. Even with the current velocity measured
559 at a variety of locations and the natural complexity inherent in a field site, both of
560 these studies found that a measure of the average silt size in the deposit was related
561 to the current velocity. For example, the data of [Ledbetter \(1986\)](#) yields a relationship
562 of $d_{ms} = 0.46U + 13.95$ ($R^2 = 0.82$) where d_{ms} is the mean silt size in μm and U is the
563 current velocity in cm/s. Here the slope, 0.46, is only slightly lower than the values
564 obtained with the laboratory study herein with the intercept falling at the low end of the
565 measured range (Fig. 12). Furthermore, in [McCave et al. \(2017\)](#), slope values from the
566 regression of $SS_{mean} = mU + b$, with SS_{mean} in μm and U in cm/s, ranged from $m = 0.59$
567 to 0.88 ($\mu\text{m}\cdot\text{s}/\text{cm}$) with intercept values between $b = 15.6$ to 7.6 (μm). These slope values
568 from [McCave et al. \(2017\)](#) are all inline with those obtained in the present flume study,
569 with the intercept values being slightly smaller than those herein.

570 The similarity in form of the relationship and the values of the regression coeffi-
571 cients between this laboratory study and the field suggest two co-supporting lines of
572 thought. The first is that the laboratory experiments reasonably reproduced advective
573 depositional sorting even at their reduced scale. The second, assuming the flume experi-
574 ments do capture the first-order physics, is that the sorting experienced in the field might
575 be an outcome of downstream advective sorting. If this is the case, then it would also be

576 reasonable to suggest that changes in the slope or intercept values along a deposit could
577 be reflective of the distanced from a suspension source location.

578 To the best of the authors' knowledge, there have been no laboratory studies that
579 have examined the relationship between SS_{mean} , U , and distance from the suspended
580 sediment source. The closest studies to this one have been the studies of Hamm et al.
581 (2009) and Hamm and Dade (2013). Both of these studies examined the dynamics of
582 silt transport in a recirculating racetrack flume. However, only Hamm and Dade (2013)
583 specifically set out to examine how the grain size distribution and SS_{mean} varied with cur-
584 rent velocities ranging from 20 to 53 cm/s. For the experiments, those authors used glass
585 microspheres with diameters in the range of 13 to 44 μm . Similar to the observations
586 here, the experiments produced both longitudinal streaks of clustered silt particles mov-
587 ing as bed load and mobile barchan shaped ripples. However, contrary to the present
588 findings, the study did not report evidence of grain size sorting within the bedforms as
589 a function of flow velocity.

590 The authors suggest that there are at least three differences between this study
591 and that of Hamm and Dade (2013) that likely account for the different outcomes of the
592 two studies with respect to sorting of silt. The first is that the velocities used herein
593 are nearly all lower than those of Hamm and Dade (2013). In the current experiments,
594 velocity ranged from 5 to 25 cm/s compared to the 20 to 53 cm/s used by Hamm and
595 Dade (2013). The second major difference is that this work used a flow through flume
596 rather than a racetrack flume, which enabled examination of the role of downstream
597 advective sorting. The third is that crushed silica silt and clay mineral was used as
598 the sediment type instead of glass microspheres. The authors expect that the first two
599 differences are the most significant in driving the differences in bed texture relationships
600 with current velocity between the two studies.

601 4.2. Modeling the trends in $SS_{mean} = SS_{mean}(x, U)$

602 This section explores the ability of the simplified model to capture the trends in the
603 experimental data, both in terms of downstream and at-a-station trends, and the model
604 is used to consider how changes in the input sediment size distribution can impact

605 $SS_{mean} = SS_{mean}(x, U)$.

606 4.2.1. Model comparison with downstream flume data

607 If the equations for α_i and $E_{s,i}$ suggested by Hamm et al. (2009) (Eqs 3 and 4),
608 and the Ferguson and Church (2004) settling velocity relation are used, then the sim-
609 plified depositional model coupled with measured data has no calibration parameters.
610 The inputs for the model include size distribution and inlet concentration (used to de-
611 fine $C_{i,0}$), the flow depth, velocity, and shear velocity, with the resulting output being
612 $f_{b,i} = f_{b,i}(x, U)$ from which SS_{mean} can be calculated. Of the measured inputs, those
613 related to the hydraulics are well constrained with little experimental or measurement
614 variability. Measured silt distributions from a deposit location under identical hydraulic
615 conditions varied little from run to run in the preliminary experiments. Nevertheless,
616 some variability was observed in the shape of measured size distribution of the silt in
617 the sediment hopper from run to run. Because the depositional model is sensitive to
618 changes in the initial grain size distribution over the depositional length of the flume,
619 the authors elected to compare the model to data from the flume using a synthetic initial
620 SS size distribution. The synthetic distribution was based on an average of the measured
621 values and assumes a normal distribution of log transformed grain sizes (as described
622 in Section 2.2).

623 The model captures the general shape of SS_{mean} with distance from the source for
624 a given velocity. The model does the best at capturing the data for the intermediate
625 velocities ($U = 10-20$ cm/s). For low velocities ($U = 5$ cm/s) the model generally
626 predicts a coarser SS_{mean} than the observation, whereas for the higher velocities it tends
627 to underestimate SS_{mean} relative to the experimental data (Fig. 13).

628 One reason for the underestimation of SS_{mean} at higher velocity might be the size
629 independent nature of α and E_s in the Hamm et al. (2009) formulations and the near
630 zero value of E_s for the particular flow conditions here. Rather than being size indepen-
631 dent, one could expect E_s to go up as grain size reduces under the consideration that
632 it is easier to entrain smaller particles. This reasoning is common in entrainment func-
633 tions for sand (e.g., Garcia and Parker, 1991), but it goes against the reasoning and data

634 presented in Hamm et al. (2009) for entrainment of particles smaller than the viscous
635 sublayer thickness. If the erosion and deposition functions did include an element of
636 size dependence, finer material would stay in suspension longer at higher flows relative
637 to large particles.

638 An attempt to improve the model to better match the experimental data was done
639 by introducing the approach of Mooneyham and Strom (2018) to model the erosion and
640 deposition terms (in place of Eqs 3 and 4). The Mooneyham and Strom (2018) approach
641 is less sophisticated than other deposition and entrainment functions, but it does provide
642 size-class-dependent net deposition and erosion functionality and it was developed for
643 suspensions of clay and silt moving over impermeable and permeable beds. However,
644 even after tuning the coefficients in the model, the method was not able to provide a
645 substantial increase in descriptive power over the model described in the *Depositional*
646 *theory* section using Eqs 3 and 4 for α and E_s .

647 It was found that the best match between the flume deposit data and the model
648 was obtained by altering the size distribution of the inlet sediment. Reasonable matches
649 between the data and the model could be obtained by increasing the mean size of the
650 inlet distribution with current velocity. For example, for the pure silt case, using $\theta_m =$
651 2.6, 2.8, 2.8, 3.2, and 3.5 for the cases of $U = 5, 10, 15, 20,$ and 25 cm/s (with $\sigma = 0.8$)
652 yielded a good fit between the model and data. An even better fit could be obtained by
653 also changing σ by up to ± 0.2 . Because the authors have no reason to expect that the
654 inlet size distribution in these experiments was a function of current velocity, a single
655 size distribution in the modelling analysis has been selected for simplicity.

656 4.2.2. Trends in SS_{mean} with velocity at a particular distance from the source

657 Similar to the experimental data, this model predicts a general steepening of the
658 $SS_{mean} = SS_{mean}(U)$ relationship (stronger sorting) with an increase in the distance from
659 the flume inlet (Fig. 1B and 12); past the length of the flume the slopes lessens as
660 coarser material is no longer available in suspension (Fig. 1B). While the trends in
661 the experimental and model slopes move in the same direction, the model predicts a
662 logarithmic form of the relation at the sampling location in the flume ($x/h = 43$ to 217

663 in Fig. 2) rather than a linear relationship. Near linear relationships are predicted farther
664 downstream once the coarser material has fully settled out, but over the length of the
665 flume the model is logarithmic.

666 The discrepancy in the shape of the relationship could be due to at least one of the
667 following two explanations. The first is that it is possible that $SS_{mean} = SS_{mean}(U)$ is truly
668 logarithmic at a given station, but that our experimental data were not able to capture the
669 underlying functionality. That is, given the experimental variability, the limited number
670 of velocities tested, and the near linear shape of the underlying log relations, the data
671 were insufficient to differentiate between a linear and log form. The second possible
672 explanation is that the model is too simplistic and either needs to account for changes in
673 the arrival rate of sediment to the bed or re-entrainment of particles that make it to the
674 bed.

675 4.2.3. *The role of input grain size distribution*

676 Modelling the downstream trends in grain size revealed that the model is depen-
677 dent on the input grain size distribution, which in natural systems can, in turn, be related
678 to the ultimate source of the sediment. The potential for the relationship between SS_{mean}
679 and current velocity to be dependent on the size distribution of the source sediment has
680 been discussed in the literature (McCave and Hall, 2006). Indeed, McCave et al. (2017)
681 attributed differences in the linear regression coefficients between SS_{mean} and U they ob-
682 served in different groupings of data to differences in the nature of the input sediment
683 and potentially to differences in the distance from the source.

684 The model is used here to examine how changes in grain size distribution of the
685 input material impact the $SS_{mean} = SS_{mean}(U)$ relationship at three different downstream
686 distances (Fig. 14). The distances from the source are given in terms of location scaled
687 with depth, x/h . The position $x/h = 217$ corresponds to the most downstream sam-
688 pling location in the flume using the experimental depth. The two additional locations
689 are roughly double that and ten times that. For a 100 m thick current, the three posi-
690 tions would correspond to 22, 50, and 200 km from the suspension source. The analysis
691 confirms that the $SS_{mean} = SS_{mean}(U)$ relationship, in an advective depositional sorting

692 environment, depends on both the distance from the input and the size distribution of
693 the input sediment. Coarsening of the input, and moving up-current so as to be closer to
694 the source, both have the effect of producing deposits that are relatively coarser. Coarsen-
695 ing of the input sediment also leads to an increase in the slope of the $SS_{mean} = SS_{mean}(U)$
696 relationship (stronger sorting) at a given distance from the input. Figure 14 also sug-
697 gests that differences in the $SS_{mean} = SS_{mean}(U)$ relationship between different source
698 material grain size distributions decreases with distance. It should be noted that changes
699 in the source sediment size distribution with time could also lead to variations SS_{mean}
700 with depth in a deposit without any change in the current velocity. Variation in source
701 sediment grain-size distribution and its potential confounding effects on interpretation
702 of SS_{mean} is also discussed in [McCave et al. \(1995\)](#) and [McCave and Hall \(2006\)](#).

703 4.3. Study context and limitations

704 4.3.1. Critical conditions

705 The presented experiments show that silt can deposit at velocities of at least 25
706 cm/s ($u_* = 1.38$ cm/s) with a d_{50} of around 35-40 microns. This value is significantly
707 larger than the critical depositional shear velocity of 0.67 cm/s suggested in [McCave
708 et al. \(2017\)](#), but is inline with the results of other laboratory experiments using silt such
709 as [Mantz \(1978\)](#), [Hamm and Dade \(2013\)](#), and [Yawar and Schieber \(2017\)](#). [Hamm and
710 Dade \(2013\)](#) saw silt deposit into barchan ripples at velocities up to 30 cm/s (0.28 Pa)
711 and [Yawar and Schieber \(2017\)](#) observed barchan ripples form at velocities of up to 55
712 cm/s (material D_{50} of 50 microns), and 40 cm/s (material D_{50} of 30 microns). Similar
713 barchan shaped bedforms have also been observed in deep sea deposits (e.g., [Hollister
714 and McCave, 1984](#)). Based on these values and observations, it seems reasonable to
715 expect that silt can actively deposit to the ocean floor under the majority of boundary
716 current conditions.

717 Deposition of clay on its own seems to achieve a critical velocity between 20 and 25
718 cm/s (0.13 - 0.19 Pa), although the inclusion of silt appears to increase this point, poten-
719 tially due to low energy areas around silt bedforms. [McCave et al. \(1995\)](#) cites a critical
720 shear velocity measured in a radial laminar flow cell by [Self et al. \(1989\)](#) for particles

721 with a diameter on 10 microns to be 0.32 cm/s. The critical shear velocity and shear
722 stress for the deposition and accumulation of clay in the experiments herein was around
723 $u_* = 1.12$ cm/s and $\tau_B = 0.13$ Pa, higher than other reported values (e.g., [McCave and](#)
724 [Swift, 1976](#); [Self et al., 1989](#); [McCave, 2008](#)). Clay deposition thresholds from the present
725 experiments are inline with those of [Schieber et al. \(2007\)](#) and [Yawar and Schieber \(2017\)](#)
726 where it was found that floccule ripples can form at velocities ranging from 10-26 cm/s.
727 These high critical conditions for silt and clay deposition, and the consolidating effect of
728 deposited clay, could lead one to conclude that only under high-magnitude events (e.g.,
729 benthic storms; [Gardner et al., 2017](#)) does erosion occur. In between such episodic events,
730 contour currents likely function as a depositional system and advectively sort material
731 that was resuspended during short-lived, high-energy events. However, the authors note
732 that direct, observation-based knowledge of such fundamental processes in the deep sea
733 is relatively limited, highlighting the importance for more field-based research of these
734 systems.

735 4.3.2. *The role of clay content in the input sediment*

736 The presence of clay in the inlet sediment had an influence on the morphology of
737 the bed that developed with time. The higher the percentage of clay, the more suppressed
738 the silty bedforms. It is possible that this suppression of bedforms might have been due
739 to the cohesive nature of the clay ([Schindler et al., 2015](#)). It is also possible that bedforms
740 were not as pronounced in beds that developed from the clay-silt mixture relative to
741 those with pure silt because of the overall reduced concentration of silt in input sediment
742 under equivalent inlet concentrations.

743 While inclusion of clay did change the bed morphology, added clay (or clay type)
744 in the input sediment did not have a strong influence on the sorting properties of the
745 silt. Both downstream and at-a-station trends in $SS_{mean} = SS_{mean}(x, U)$ were relatively
746 insensitive to the amount of clay in the input sediment. This behaviour can be seen in
747 [Figure 12](#) and [Table 3](#) where slope and intercept values in the regression of $SS_{mean} =$
748 $mU + b$ show little variability with the silt to clay ratio. The authors expect this outcome
749 is a reflection of the little influence the suspended clay has on advective depositional

750 sorting in these experiments.

751 The presence of clay has the possibility of influencing sorting of silt through at least
752 three mechanisms. The first would be through binding of clay and silt particles into flocs
753 within the suspension, thereby altering the settling velocity of both fractions. While the
754 effect on the silt settling velocity was small relative to the effect of the silt on the clay
755 floc settling velocity, [Tran and Strom \(2017\)](#) did find evidence of the silt settling velocity
756 being slightly reduced if it is traveling in flocs rather than unflocculated. If sorting in the
757 deposit is primarily an outcome of advective depositional sorting, then the binding of silt
758 size material in mud flocs within the suspension, thereby altering the settling velocity
759 of the silt, would be the primary way in which the presence of clay could impact the
760 sorting of silt.

761 This study looked for the occurrence of clay-silt floc binding in suspension and on
762 the bed using the camera system explained in [Rouhnia and Strom \(2017\)](#) and [Mooney-
763 ham and Strom \(2018\)](#) and in the mixing tank experiments outlined in the methods. In
764 all samples, no indication of binding of the two fractions in suspension was evident. The
765 silt existed as independent grains and the clay in visible aggregates roughly the same
766 size as the silt or below the resolution of the camera ($\approx 15 \mu\text{m}$); no large, low-density
767 flocs such as those in [Tran and Strom \(2017\)](#) were found. The lack of silt binding in
768 mud flocs within the present experiments suggests that additional work should be done
769 in the future to better constrain the control that flocculation may place in downstream
770 advective sorting of silt.

771 The second way in which clay could have impacted the depositional sorting of silt
772 is through alterations to the deposition and re-entrainment rates (α and E_s in the model).
773 If deposited clay provided a measure of cohesion, it might lead to increased retention
774 of fine silt particles that might have otherwise been resuspended back up into the flow
775 leading to less-well-sorted silt. While such a situation seems plausible, the experiments
776 do not support this line of reasoning. There was additional variability in the measured
777 deposit silt size distribution for the runs with clay, but the overall slope and intercept
778 regression coefficients from the runs with clay were similar to those from the pure silt
779 runs regardless of the amount of clay added. The similar slope of the regression, and the

780 near zero value for E_s , suggest that cohesion between the clay and silt near the boundary
781 did not strongly influence the resuspension rate.

782 A third way that clay could have impacted sorting of silt in the deposit, and one
783 that is not captured by the model, is through clay and silt interactions within the bed
784 load layer.

785 4.3.3. *Bed load*

786 Both the SS hypothesis and the depositional model assume that particles do not
787 move along the bed once they are deposited; i.e., no bed load transport. However, bed
788 load was apparent in all silt and silt-clay experiments at or above $U = 15$ cm/s. It is this
789 bed load that resulted in the creation of ripples that would migrate downstream with or
790 without sediment in suspension. The pure silt ripples that formed in this study's non-
791 recirculating flume closely resembled in size and shape the ripples that formed in the
792 racetrack flume experiments of [Yawar and Schieber \(2017\)](#) (at 25 cm/s) and [Hamm and](#)
793 [Dade \(2013\)](#) (at 20 cm/s). The silt-clay ripples were also similar in size, but contained
794 some clay clumps. Similar silty clay ripples have also been observed in the field ([Hollister](#)
795 [and McCave, 1984](#)).

796 While the movement of clay particles along the bed was observed in the pure
797 clay experiments, the formation of migrating barchan ripples composed purely of clay
798 floccules was not seen, as was observed in [Schieber et al. \(2007\)](#) for similar current
799 velocities. A potential reason for the lack of migrating clay bedforms in the present
800 study might be the relatively short length of the flume. The advective length scale of
801 clay is significant, and it maybe that more flume length would have been needed to
802 deposit sufficient clay material at those velocities to allow for the formation of larger
803 clay floccules and migrating barchan clay ripples.

804 Regardless, observations of bed load and bedforms in these experiments and oth-
805 ers all indicate that sediment deposited to the bed does have the ability to transport
806 downstream below a critical shear stress for re-entrainment. This is acknowledged in
807 the SS hypothesis. However, it is suggested that bed load and selective erosion in mud
808 is diminished due to cohesion in the bed. Leaving selective deposition as the key sorting

809 mechanism (McCave, 2008). The implication of bed load transport of deposited grains
810 is that particles that originally deposited at one location under advective sorting could
811 move to another location over long enough periods of time before becoming buried and
812 incorporated into the sedimentary record at a particular location. On its own, such
813 movement could alter the at-a-station relationship between SS_{mean} and U such as those
814 examined in this study. Furthermore, having bed load movement of both clay and silt
815 size material could further complicate the relationships. In studying deposits generated
816 from mixtures of silt and clay moving as bed load, Yawar and Schieber (2017) found that
817 the smaller fraction of silt ($d = 1-30 \mu\text{m}$, a portion of which is part of the SS fraction) sep-
818 arated from the broader silt fraction, bound with the clay floccules, and then deposited
819 with the clay floccules.

820 Bed load transport in general, along with the potential for clay-silt interaction
821 within the bed load layer, could complicate the simple advective depositional sorting
822 relationships explored and modelled in this study. Bed load transport is not accounted
823 for in the model, and it is possible that the short length of the flume and short run
824 time of the experiments minimized effects due to bed load transport and potential in-
825 teractions between the clay and silt in the bed load layer. It must be acknowledged that
826 neither bed load motion over long distances nor any shift in deposit location for the silt
827 fraction between 1 and 30 μm due to transport within clay floccules is accounted for.
828 Furthermore, neither these experiments or model account for the winnowing effects of
829 erosion. As such, caution should be used when seeking to extend the present findings
830 to more complicated field settings.

831 5. Conclusions

832 This study used a laboratory experiment and simple suspended sediment transport
833 theory to investigate the relationship between mean sortable silt in a deposit, SS_{mean} ,
834 and average current velocity at the time of deposition in an advectively sorted system.
835 The velocity used in the study ranged from 5 to 25 cm/s, velocities typical of deep-sea
836 environments. Under these conditions, the laboratory currents were largely depositional.
837 The relationship between SS_{mean} and velocity was examined both at a particular distance

838 from the input of suspended sediment (at a station) and as a function of total distance
839 from the sediment input (downstream). Sediment used in the experiments consisted
840 of crushed silica in the silt size range and different mixtures of the silica silt with clay
841 minerals. The combination of the experimental methods and materials led to advective
842 depositional sorting where silt sizes in the deposit fine with distance from the input and
843 coarsen with increasing velocity and current thickness.

844 From the experiments, it was found that SS_{mean} was linearly related to U at a
845 particular location in the flume; this outcome is similar to the field calibration of [McCave
846 et al. \(2017\)](#). Regression between SS_{mean} in microns and U in cm/s produced fits with
847 R^2 values between 0.7 and 0.94 and coefficient values similar to those from the field,
848 even though the scales of the two studies are very different. In general, the slope of the
849 $SS_{mean} = SS_{mean}(U)$ regression increased, while the intercept decreased, with distance
850 from the input in both experiments and theory over the scaled length of the flume.

851 A model for SS_{mean} in the deposit was developed using simple theory. For the
852 experimental conditions, the model was able to reasonably describe the size distribution
853 of silt in the deposit as a function of the input grain size distribution, the distance from
854 the input, velocity, and current thickness. Based on this, the model was extrapolated to
855 distances of up to ten times the length of the flume (or out to 200 km for a 100 m thick
856 current). Doing so enables an illustration of the impact of distance from the source and
857 source grain size distribution on the $SS_{mean} = SS_{mean}(U)$ relationship for a broader range
858 of conditions than those explored experimentally.

859 Both the experiments and theory demonstrated the importance of the thickness of
860 the current, h , in the sorting process. More specifically, the theory shows that the amount
861 of silt in size fraction, i , within a deposit is strongly dependent on the ratio x/L_i ; where
862 x is the distance from the source and L_i is the advective length scale $L_i = hU/(\alpha w_{s,i})$.
863 This shows that that L_i is linearly dependent on both U and h . Doubling either will
864 produce a doubling of L_i .

865 This study shows that silt can advectively sort under depositional conditions, and
866 it highlights how the distance from the input, flow thickness, and changes in the input
867 grain size can alter the relationship. The similarity in the linearity between SS_{mean} and

868 U and the regressed slope and intercept values between the laboratory and field suggest
869 that the field data of [McCave et al. \(2017\)](#) might have also been the outcome of advective
870 sorting.

871 While the study explores advective depositional sorting of suspensions containing
872 silt and clay, neither the theory nor experiments account for complicating interactions in
873 these two size fractions that can arise due to flocculation. The experiments and model
874 also do not account for winnowing due to erosion or long-range bed load transport of silt
875 size grains that, if it occurs, has the potential to also complicate the $SS_{mean} = SS_{mean}(x, U)$
876 relationship.

877 **Acknowledgements**

878 Funding for this work was provided by American Chemical Society-Petroleum Re-
879 search Fund-New Directions grant 57811-ND awarded to BWR and KS. Data associated
880 with this study can be obtained from GitHub at github.com/FluidSedDynamics, or by
881 contacting the corresponding author (strom@vt.edu). We are grateful for the helpful re-
882 views and critiques provided by Juergen Scheiber, I. N. McCave, an anonymous reviewer,
883 and associate editor Jaco Baas.

884 **References**

- 885 Bianchi, G. G., Hall, I. R., McCave, I. N., and Joseph, L. (1999). Measurement of the
886 sortable silt current speed proxy using the Sedigraph 5100 and Coulter Multisizer II:
887 precision and accuracy. *Sedimentology*, 46(6):1001–1014.
- 888 Broecker, W. S., Peacock, S. L., Walker, S., Weiss, R., Fahrback, E., Schroeder, M., Mikola-
889 jewicz, U., Heinze, C., Key, R., Peng, T.-H., and Rubin, S. (1998). How much deep water
890 is formed in the southern ocean? *Journal of Geophysical Research: Oceans*, 103(C8):15833–
891 15843.
- 892 Charru, F. and Hinch, E. J. (2006). Ripple formation on a particle bed sheared by a
893 viscous liquid. part 1. steady flow. *Journal of Fluid Mechanics*, 550:111–121.

- 894 Dixit, J. G., Mehta, A. J., and Partheniades, E. (1982). Redepositional properties of co-
895 hesive sediments deposited in a long flume. Report UFL/COEL-82/002, Coastal &
896 Oceanographic Engineering Department, University of Florida, Gainesville, FL USA.
- 897 Einstein, H. A. and Krone, R. B. (1962). Experiments to determine modes of cohesive
898 sediment transport in salt water. *Journal of Geophysical Research*, 67(4):1451–1461.
- 899 Ferguson, R. and Church, M. (2004). A simple universal equation for grain settling
900 velocity. *Journal of Sedimentary Research*, 74(6):933–937.
- 901 Garcia, M. and Parker, G. (1991). Entrainment of bed sediment into suspension. *Journal*
902 *of Hydraulic Engineering*, 117(4):414–435.
- 903 García, M. H. (2008). *Sediment Transport and Morphodynamics. Sedimentation Engineering*,
904 chapter 2 Sediment Transport and Morphodynamics, pages 21–163. ASCE Manuals
905 and Reports on Engineering Practice No. 110. ASCE.
- 906 Gardner, W. D., Tucholke, B. E., Richardson, M. J., and Biscaye, P. E. (2017). Benthic
907 storms, nepheloid layers, and linkage with upper ocean dynamics in the western North
908 Atlantic. *Marine Geology*, 385:304 – 327.
- 909 Hamm, N. T. and Dade, W. B. (2013). A laboratory study of dynamic sorting of fine,
910 non-cohesive particles by steady, unidirectional currents. *Marine Geology*, 336:215 –
911 222.
- 912 Hamm, N. T., Dade, W. B., and Renshaw, C. E. (2009). Fine particle deposition to initially
913 starved, stationary, planar beds. *Sedimentology*, 56(7):1976–1991.
- 914 Haralampides, K., McCorquodale, J. A., and Krishnappan, B. G. (2003). Deposition
915 properties of fine sediment. *Journal of Hydraulic Engineering*, 129(3):230–234.
- 916 Heezen, B. C., Hollister, C. D., and Ruddiman, W. F. (1966). Shaping of the continental
917 rise by deep geostrophic contour currents. *Science*, 152(3721):502–508.
- 918 Hollister, C. D. and McCave, I. N. (1984). Sedimentation under deep-sea storms. *Nature*,
919 309(5965):220–225.

- 920 Jarvie, D. M., Hill, R. J., Ruble, T. E., and Pollastro, R. M. (2007). Unconventional shale-
921 gas systems: The Mississippian Barnett Shale of north-central Texas as one model for
922 thermogenic shale-gas assessment. *AAPG Bulletin*, 91(4):475–499.
- 923 Kleiven, H. K. F., Hall, I., McCave, I., Knorr, G., and Jansen, E. (2011). Coupled deep-
924 water flow and climate variability in the middle Pleistocene North Atlantic. *Geology*,
925 39(4):343–346.
- 926 Knutz, P. (2008). Paleooceanographic significance of contourite drifts. *Developments in*
927 *Sedimentology*, 60:511–535.
- 928 Lau, Y. L. and Krishnappan, B. G. (1992). Size distribution and settling velocity of cohe-
929 sive sediments during settling. *Journal of Hydraulic Research*, 30(5):673–684.
- 930 Law, B., Hill, P., Milligan, T., Curran, K., Wiberg, P., and Wheatcroft, R. (2008). Size
931 sorting of fine-grained sediments during erosion: Results from the western Gulf of
932 Lions. *Continental Shelf Research*, 28(15):1935 – 1946.
- 933 Ledbetter, M. T. (1986). A late pleistocene time-series of bottom-current speed in the
934 Vema Channel. *Palaeogeography, Palaeoclimatology, Palaeoecology*, 53(1):97 – 105.
- 935 Mantz, P. A. (1978). Bedforms produced by fine, cohesionless, granular and flakey sedi-
936 ments under subcritical water flows. *Sedimentology*, 25(1):83–103.
- 937 McCave, I. and Andrews, J. (2019). Distinguishing current effects in sediments delivered
938 to the ocean by ice. I. Principles, methods and examples. *Quaternary Science Reviews*,
939 212:92 – 107.
- 940 McCave, I., Thornalley, D., and Hall, I. (2017). Relation of sortable silt grain-size to deep-
941 sea current speeds: Calibration of the ‘mud current meter’. *Deep Sea Research Part I:*
942 *Oceanographic Research Papers*, 127(Supplement C):1 – 12.
- 943 McCave, I. N. (2008). Size sorting during transport and deposition of fine sediments:
944 Sortable silt and flow speed. In *Developments in Sedimentology*, volume 60, chapter 8,
945 pages 121–142. Elsevier.

- 946 McCave, I. N. and Hall, I. R. (2006). Size sorting in marine muds: Processes, pit-
947 falls, and prospects for paleoflow-speed proxies. *Geochemistry, Geophysics, Geosystems*,
948 7(10):Q10N05.
- 949 McCave, I. N., Manighetti, B., and Robinson, S. G. (1995). Sortable silt and fine sediment
950 size/composition slicing: Parameters for palaeocurrent speed and palaeoceanography.
951 *Paleoceanography*, 10(3):593–610.
- 952 McCave, I. N. and Swift, S. A. (1976). A physical model for the rate of deposition of
953 fine-grained sediments in the deep sea. *GSA Bulletin*, 87(4):541–546.
- 954 Mooneyham, C. and Strom, K. (2018). Deposition of suspended clay to open and sand-
955 filled framework gravel beds in a laboratory flume. *Water Resources Research*, 54:323–
956 344.
- 957 Niño, Y., Lopez, F., and Garcia, M. (2003). Threshold for particle entrainment into sus-
958 pension. *Sedimentology*, 50(2):247–263.
- 959 Partheniades, E. (2006). *Engineering Properties and Hydraulic Behavior of Cohesive Sediments*.
960 CRC Press.
- 961 Rebesco, M., Hernández-Molina, F. J., Rooij, D. V., and Wåhlin, A. (2014). Contourites
962 and associated sediments controlled by deep-water circulation processes: State-of-the-
963 art and future considerations. *Marine Geology*, 352:111 – 154.
- 964 Richardson, M. J., Weatherly, G. L., and Gardner, W. D. (1993). Benthic storms in the
965 Argentine Basin. *Deep Sea Research Part II: Topical Studies in Oceanography*, 40(4):975 –
966 987.
- 967 Rouhnia, M. and Strom, K. (2017). Sedimentation from buoyant muddy plumes in the
968 presence of interface mixing: An experimental study. *Journal of Geophysical Research:*
969 *Oceans*, 122:2652–2670.
- 970 Saffman, P. G. (1965). The lift on a small sphere in a slow shear flow. *Journal of Fluid*
971 *Mechanics*, 22:385–400.

- 972 Schieber, J. (1998). Sedimentary features indicating erosion, condensation, and hiatuses
973 in the Chattanooga Shale of central Tennessee: relevance for sedimentary and strati-
974 graphic evolution. In Schieber, J., Zimmerle, W., and Sethi, P., editors, *Shales and Mud-*
975 *stones, Basin Studies, Sedimentology and Paleontology*, pages 187–215. Schweizerbart'sche
976 Verlagsbuchhandlung, Stuttgart.
- 977 Schieber, J. (2011). Reverse engineering mother nature – shale sedimentology from an
978 experimental perspective. *Sedimentary Geology*, 238(1-2):1 – 22.
- 979 Schieber, J., Southard, J. B., and Thaisen, K. (2007). Accretion of mudstone beds from
980 migrating floccule ripples. *Science*, 318:1760–1763.
- 981 Schindler, R. J., Parsons, D. R., Ye, L., Hope, J. A., Baas, J. H., Peakall, J., Manning,
982 A. J., Aspden, R. J., Malarkey, J., Simmons, S., Paterson, D. M., Lichtman, I. D., Davies,
983 A. G., Thorne, P. D., and Bass, S. J. (2015). Sticky stuff: Redefining bedform prediction
984 in modern and ancient environments. *Geology*, 43(5):399–402.
- 985 Self, R. F. L., Nowell, A. R. M., and Jumars, P. A. (1989). Factors controlling critical shears
986 for deposition and erosion of individual grains. *Marine Geology*, 86:181–199.
- 987 Slatt, R. M. (2011). Important geological properties of unconventional resource shales.,
988 *Open Geosciences*, 3(4):435–448.
- 989 Teeter, A. M. (1997). Size-dependant erosion of two silty-clay sediment mixtures. Report,
990 Waterways Experiment Station, Vicksburg, MS, USA.
- 991 Thornalley, D. J. R., Blaschek, M., Davies, F. J., Praetorius, S., Oppo, D. W., McManus, J. F.,
992 Hall, I. R., Kleiven, H., Renssen, H., and McCave, I. N. (2013). Long-term variations in
993 Iceland–Scotland overflow strength during the Holocene. *Climate of the Past*, 9(5):2073–
994 2084.
- 995 Tran, D. and Strom, K. (2017). Suspended clays and silts: Are they independent or
996 dependent fractions when it comes to settling in a turbulent suspension? *Continental*
997 *Shelf Research*, 138:81 – 94.

998 Yawar, Z. and Schieber, J. (2017). On the origin of silt laminae in laminated shales.
999 *Sedimentary Geology*, 360(Supplement C):22–34.

Sediment	Inlet Concentration, C_0 [mg/L]	Velocity, U [cm/s]
Pure Silt	374-1660	5, 10, 15, 20, 25
Pure Clay	482-2070	5, 10, 15, 20, 25
Clay & Silt (1:1 ratio)	328-1654	5, 10, 15, 20, 25
Clay & Silt (2:1 ratio)	393-1871	5, 10, 15, 20, 25

Table 1: Experimental Matrix

U [cm/s]	u_* [m/s]	τ_B [Pa]	δ [μm]	S [-]	u_*/w_s			τ^*/τ_{cr}^*		
					$d_{10\mu\text{m}}$	$d_{30\mu\text{m}}$	$d_{60\mu\text{m}}$	$d_{10\mu\text{m}}$	$d_{30\mu\text{m}}$	$d_{60\mu\text{m}}$
5	0.003	0.01	1632	0.002	49.4	5.6	1.5	0.2	0.2	0.2
10	0.006	0.04	930	0.012	86.8	9.8	2.6	0.6	0.5	0.5
15	0.009	0.08	641	0.038	125.8	14.3	3.7	1.2	1.1	1.0
20	0.012	0.13	491	0.085	164.3	18.6	4.9	2.0	1.8	1.7
25	0.014	0.19	413	0.143	195.6	22.2	5.8	2.9	2.6	2.4

Table 2: Conditions at a given flow velocity. δ is the thickness of the viscous sublayer. Values of u_*/w_s and τ^*/τ_{cr}^* are given for representative grain sizes of 10, 30, and 60 μm .

Sediment	Station, L [m]	Slope [$\mu\text{m-s/cm}$]	Intercept [μm]	R^2
Pure Silt	1.52	0.69	24.0	0.96
Pure Silt	3.05	0.85	16.4	0.99
Pure Silt	4.57	0.76	16.1	0.89
Pure Silt	6.10	0.82	13.6	0.93
Pure Silt	7.62	0.88	11.8	0.99
Silt & Clay 1:1	1.52	0.40	25.9	0.84
Silt & Clay 1:1	3.05	0.73	16.0	0.90
Silt & Clay 1:1	4.57	0.70	17.6	0.94
Silt & Clay 1:1	6.10	0.89	14.3	0.99
Silt & Clay 1:1	7.62	0.34	20.6	0.69
Silt & Clay 1:2	1.52	0.44	22.8	0.88
Silt & Clay 1:2	3.05	0.33	23.0	0.64
Silt & Clay 1:2	4.57	0.70	16.2	0.98
Silt & Clay 1:2	6.10	0.82	13.0	1.00
Silt & Clay 1:2	7.62	0.74	13.2	1.00
All	1.52	0.54	23.8	0.70
All	3.05	0.66	18.1	0.81
All	4.57	0.73	16.5	0.91
All	6.10	0.82	13.9	0.94
All	7.62	0.80	13.2	0.94

Table 3: Linear regression coefficients for $SS_{mean} = SS_{mean}(U)$. Regression slope and intercept values are given for individual sediment times (e.g., Pure Silt) and for the combination of all data from different sediment input (All). R^2 values of 1 indicate conditions where only two points were available due to the lack of deposition in some silt and clay runs.

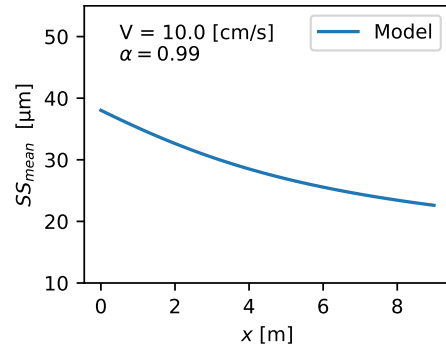


Figure 1: Solution of the simplified model for $SS_{mean} = SS_{mean}(x, U = 10 \text{ cm/s})$ based on Eqs 9 and 2

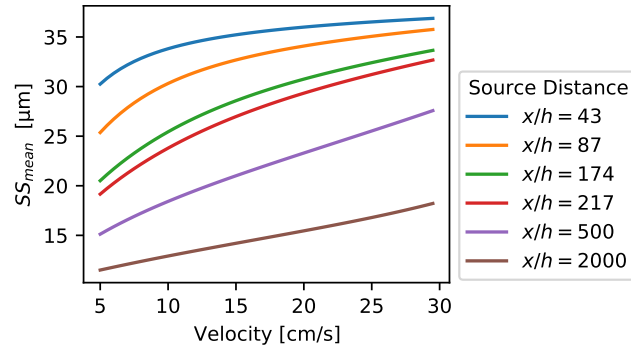


Figure 2: Solution of the simplified model for $SS_{mean} = SS_{mean}(x, U)$ based on Eqs 9 and 2. The each line shows the relationship between SS_{mean} and U at a particular distance from the source or flume inlet. The first four lines ($x/h = 43, 87, 174,$ and 217) correspond to the sampling locations in the flume. The last two represent a hypothetical extension of the flume by a factor of 2 and 10 ($x/h = 500$ and 2000).

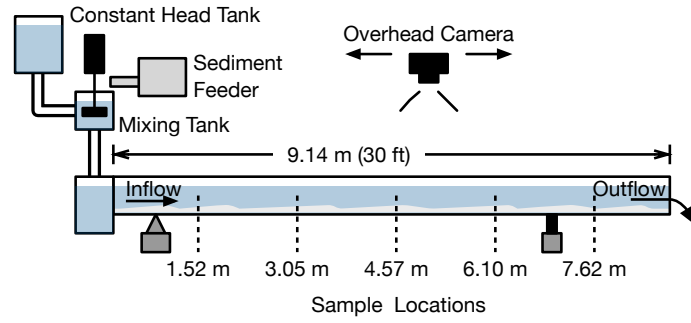


Figure 3: Experimental Setup.

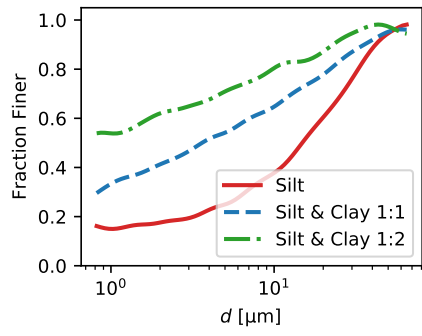


Figure 4: Initial grain size distributions for the three mixtures that included silt.

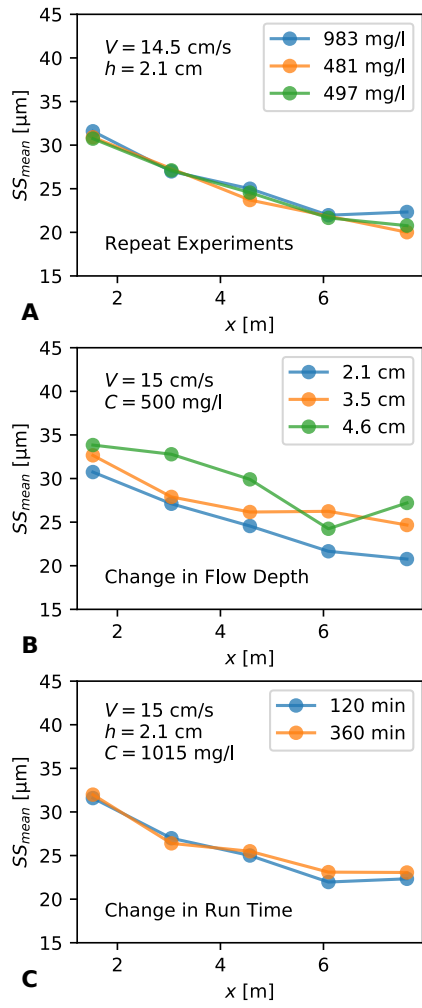


Figure 5: The distribution of SS_{mean} down channel for the preliminary runs. (A) repeat experiments no change in experimental conditions except the inlet concentration, (B) changes in flow depth, h , only, and (C) changes in experimental runtime.

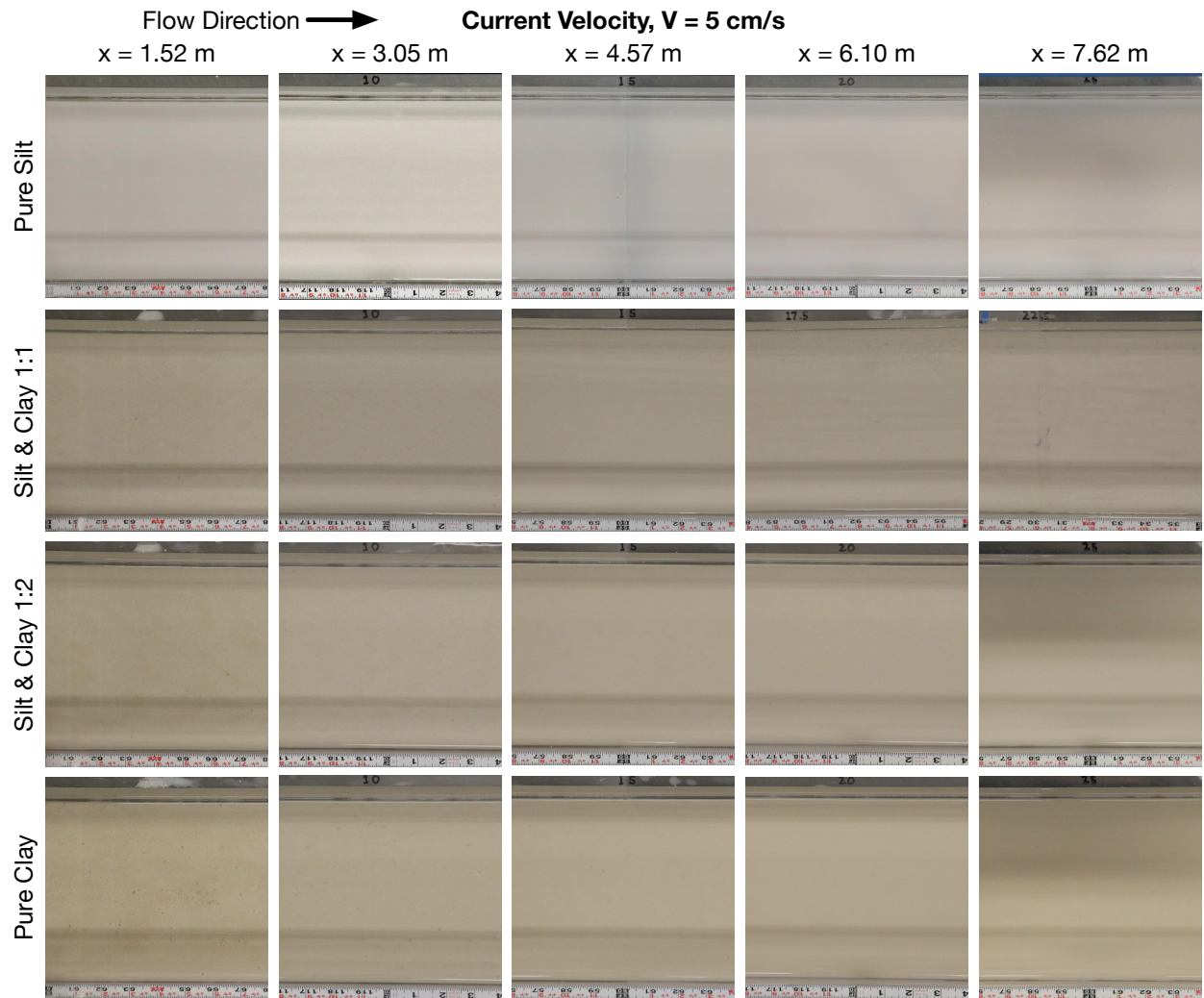


Figure 6: Images of the bed at the end of each of the $U = 5$ cm/s runs. x is the distance downstream from the inlet.

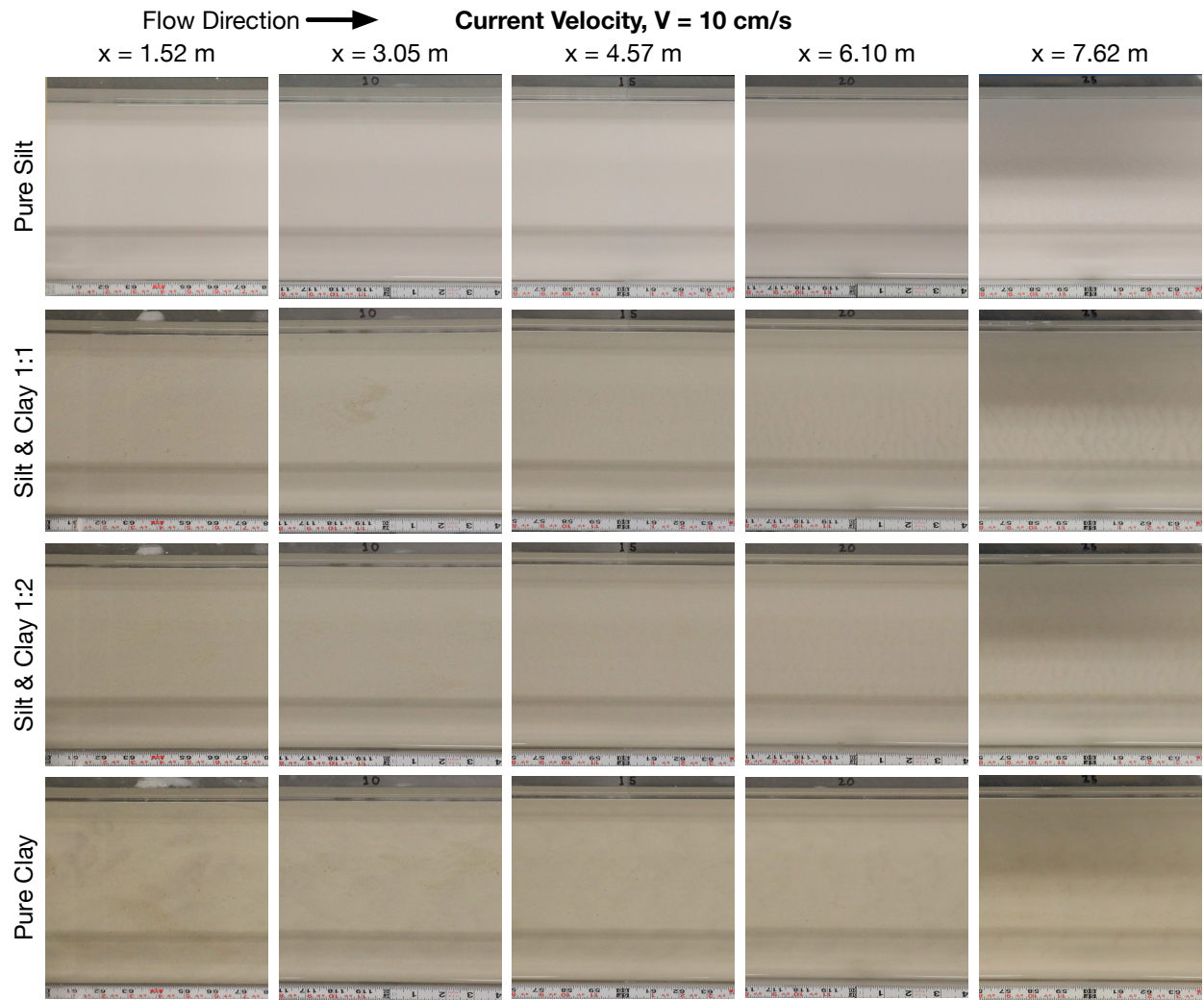


Figure 7: Images of the bed at the end of each of the $U = 10$ cm/s runs. x is the distance downstream from the inlet.

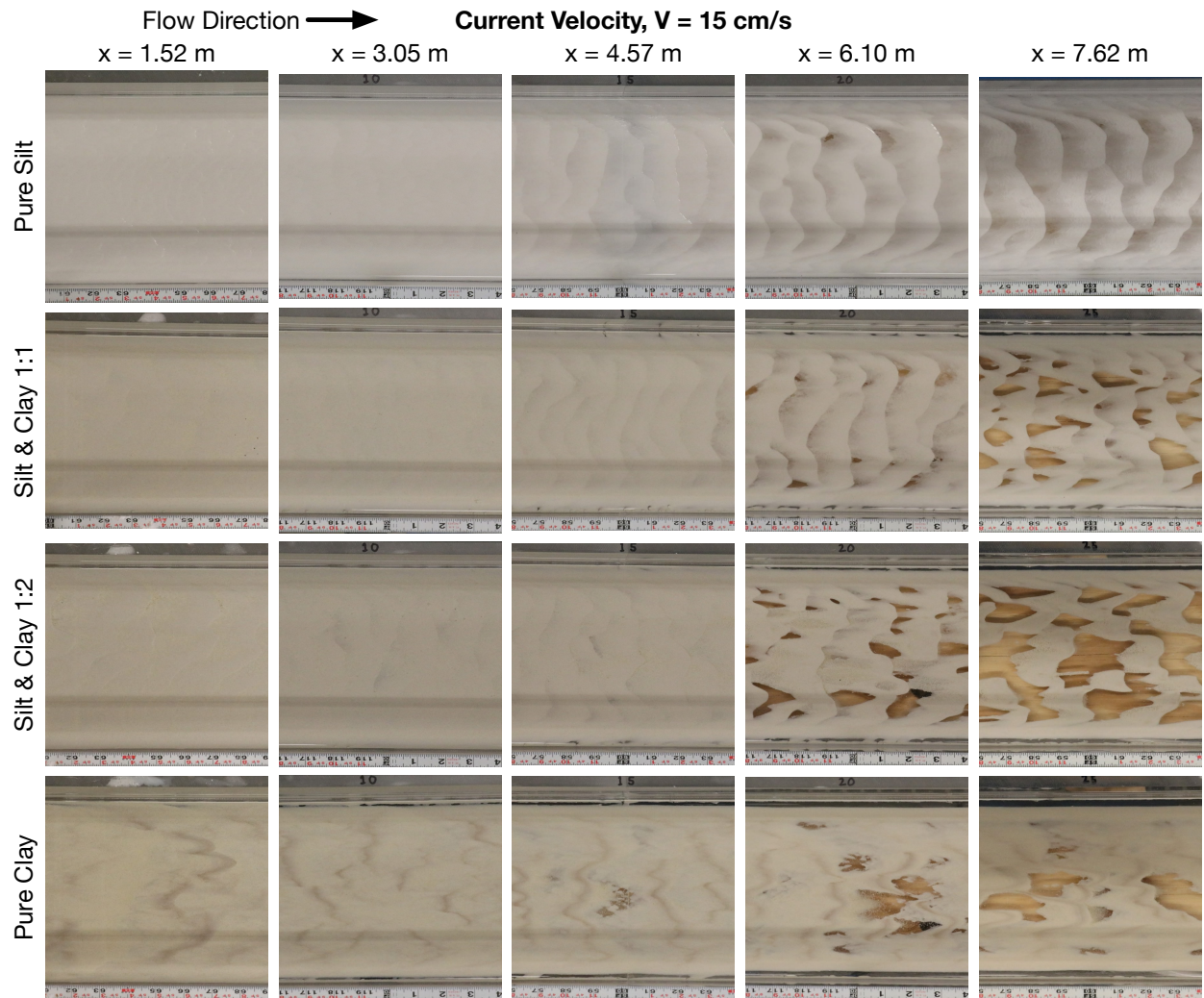


Figure 8: Images of the bed at the end of each of the $U = 15$ cm/s runs. x is the distance downstream from the inlet.

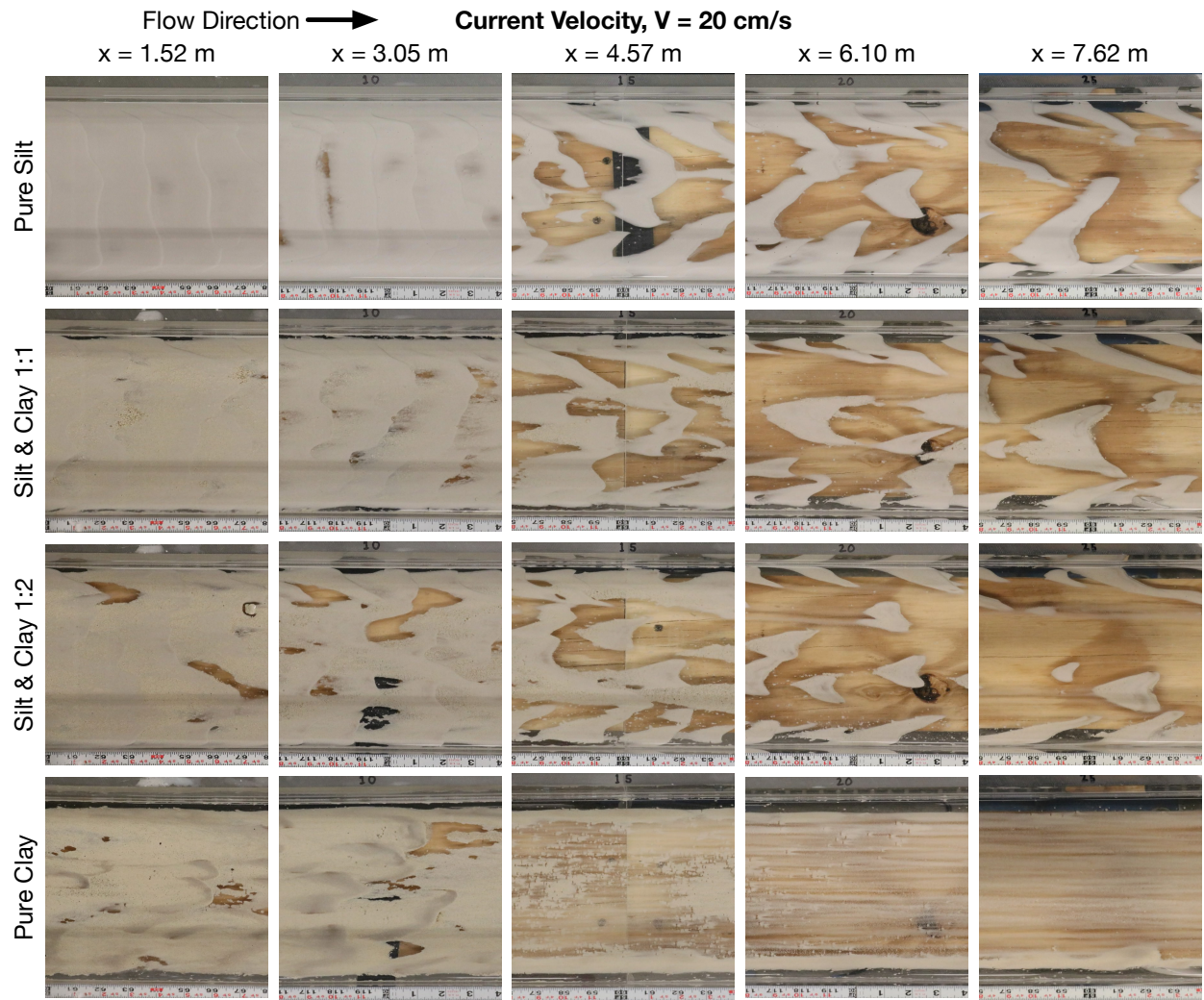


Figure 9: Images of the bed at the end of each of the $U = 20$ cm/s runs. x is the distance downstream from the inlet.

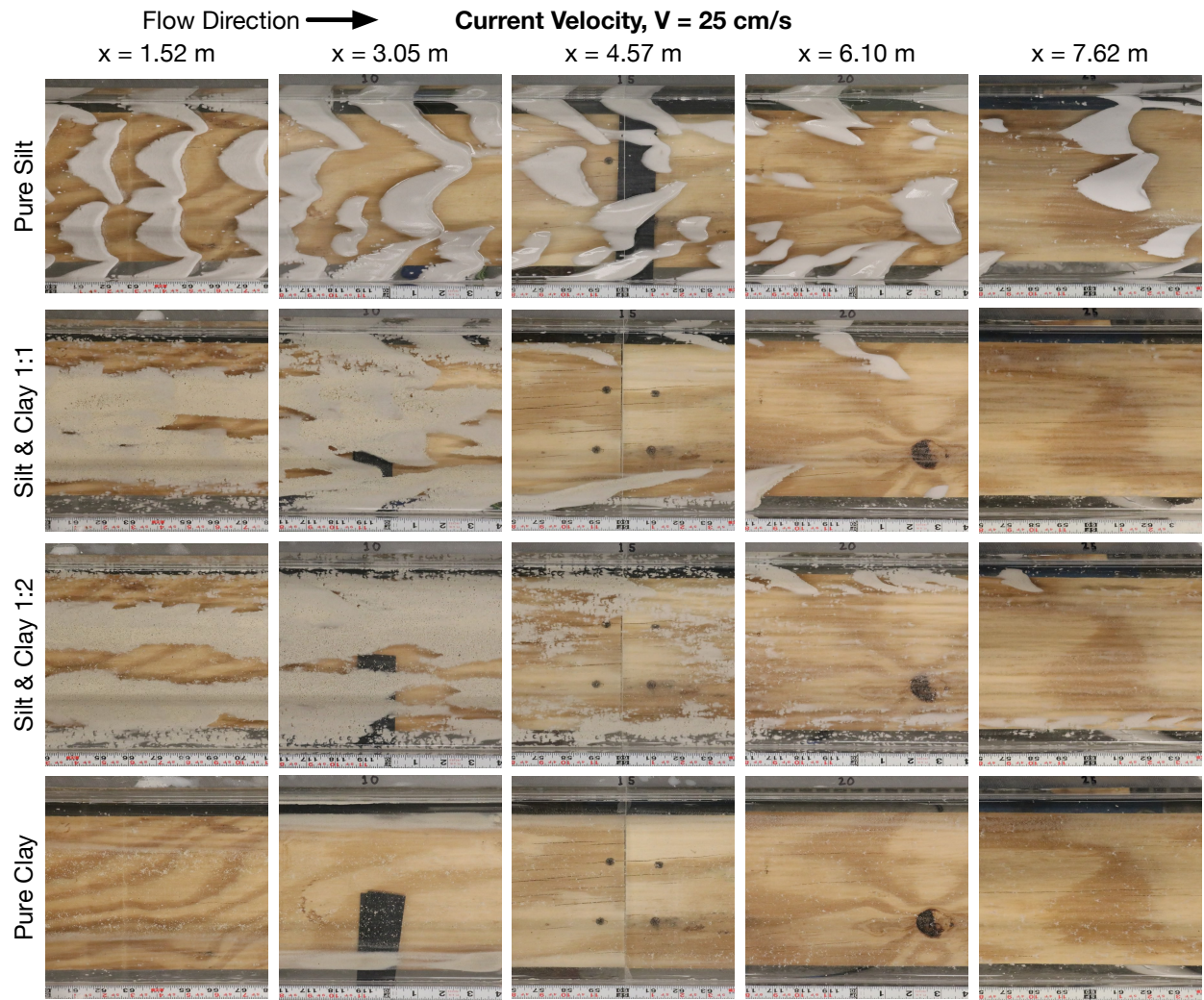


Figure 10: Images of the bed at the end of each of the $U = 25$ cm/s runs. x is the distance downstream from the inlet.

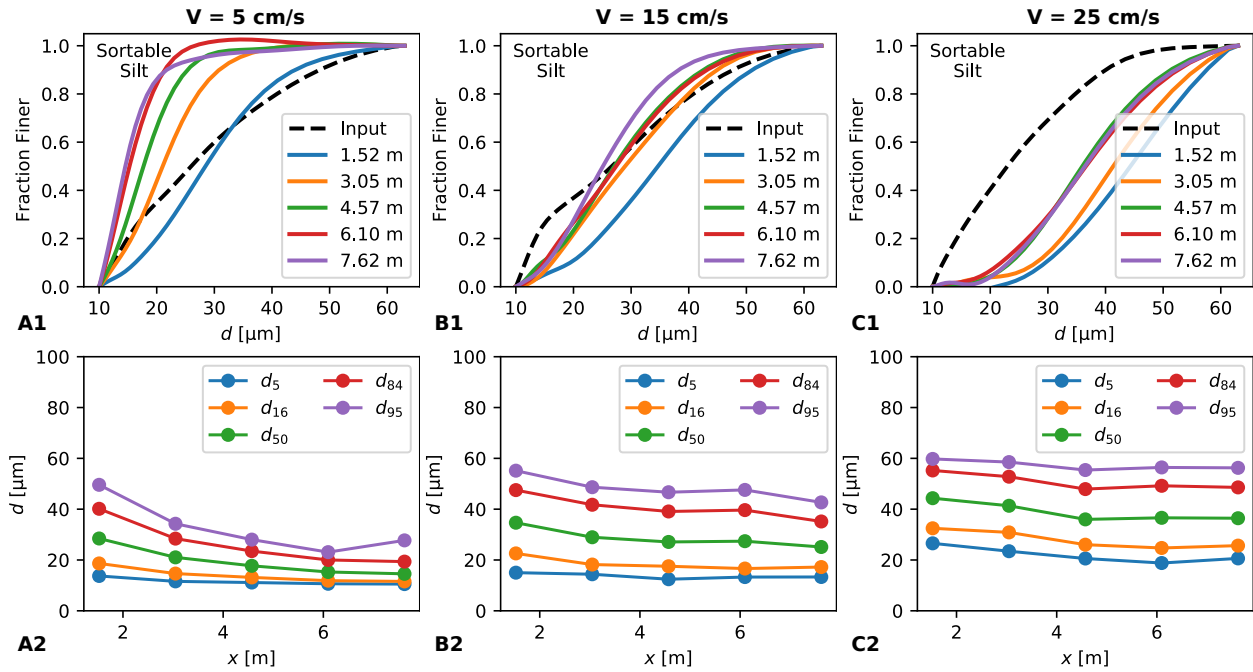


Figure 11: Downstream trends in the distribution of the sortable silt fraction for (A) $U = 5$ cm/s, (B) $U = 15$ cm/s, and (C) $U = 25$ cm/s; all plots are for runs with Pure Silt. At all velocities, the top row shows the cumulative distributions of the SS fraction and the bottom row shows the distribution statistics as a function of distance down channel from the inlet.

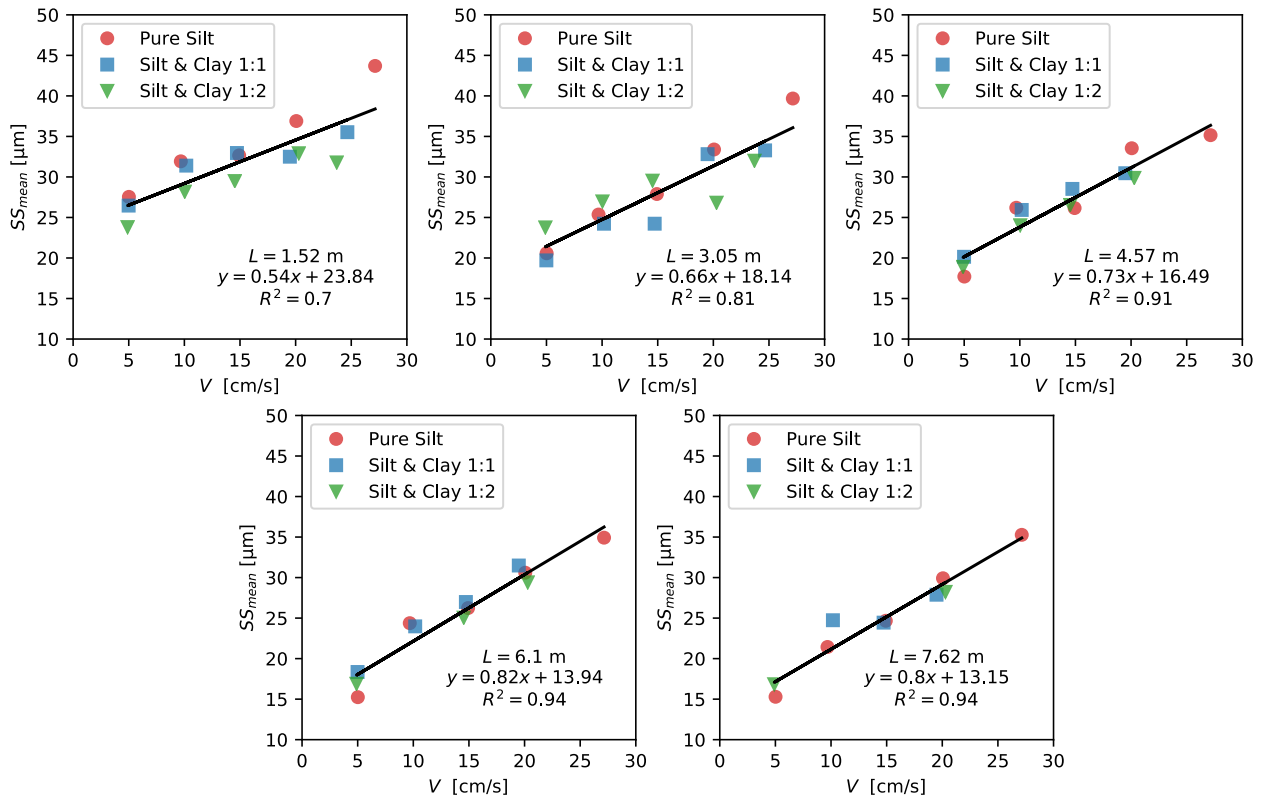


Figure 12: Regression between SS_{mean} and current velocity at each of the five sampling locations. L is the distance between the sediment input location and the sample location.

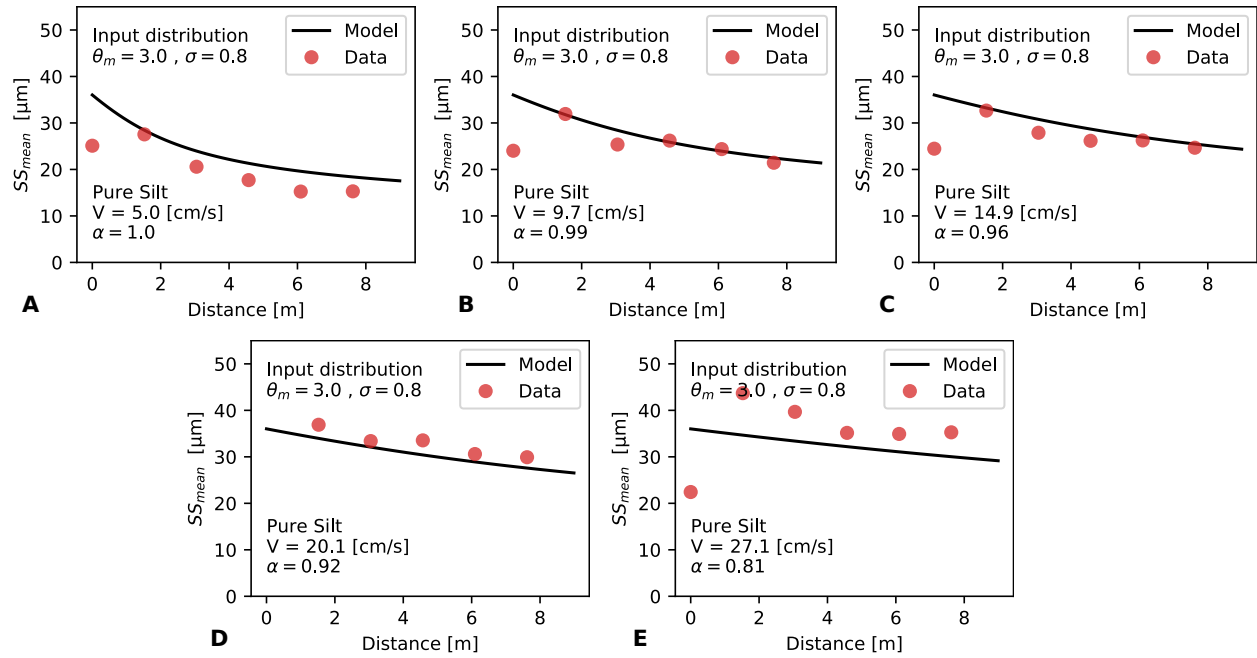


Figure 13: Comparison between the model and observations for low, moderate, and high velocities. SS_{mean} at $x = 0$ m corresponds to the inlet sample SS_{mean} .

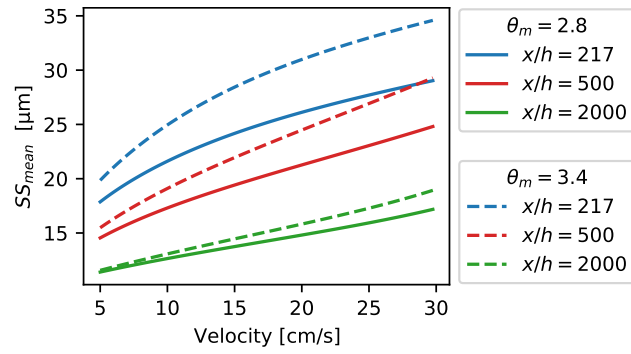


Figure 14: Model output showing the role of input grain size distribution on SS_{mean} trends with distance from input and velocity. Colors represent distance from input. The two different line types represent the two different sediment input distributions. Input 1 (solid lines) is for a distribution with $\theta_m = 2.8$ ($16 \mu\text{m}$) and input 2 (dashed lines) has $\theta_m = 3.4$ ($30 \mu\text{m}$); both have $\sigma = 0.8$.